Natural Resources Canada
Ressources naturelles Canada

Geology and U-Pb geochronology of low-grade mafic rocks from the St. Cyr klippe and a marble from the footwall, Canadian Cordillera, Yukon

S.J. Isard., J.A. Gilotti, W.C. McClelland, M.B. Petrie, and C.R. van Staal

Geological Survey of Canada
Current Research 2016-1

2016

Canada

Geological Survey of Canada
Current Research 2016-1

Geology and U-Pb geochronology of low-grade mafic rocks from the St. Cyr klippe and a marble from the footwall, Canadian Cordillera, Yukon

S.J. Isard., J.A. Gilotti, W.C. McClelland,
M.B. Petrie, and C.R. van Staal

2016

ISSN 1701-4387
ISBN 978-0-660-04031-8
Catalogue M44-2016/1E-PDF
doi:10.4095/297474

A copy of this publication is also available for reference in depository libraries across Canada through access to the Depository Services Program's Web site at http://dsp-psd.pwgsc.gc.ca

This publication is available for free download through GEOSCAN http://geoscan.nrcan.gc.ca

Recommended citation

Isard, S.J., Gilotti, J.A., McClelland, W.C., Petrie, M.B., and van Staal, C.R., 2016. Geology and U-Pb geochronology of low-grade mafic rocks from the St. Cyr klippe and a marble from the footwall, Canadian Cordillera, Yukon; Geological Survey of Canada, Current Research 2016-1, 22 p. doi:10.4095/297474

Critical review

J. Ryan

Authors

S.J. Isard (sierra.isard@gmail.com)
J.A. Gilotti (jane-gilotti@uiowa.edu)
W.C. McClelland (bill-mcclelland@uiowa.edu)
M.B. Petrie (mbpetrie@gmail.com)
Department or Earth and Environmental Sciences
University of Iowa
Iowa City, Iowa 52240, U.S.A.

C.R. van Staal (cees.vanstaal@canada.ca)
Geological Survey of Canada
1500-605 Robson Street,
Vancouver, British Columbia
V6B 5J3

Correction date:

Geology and U-Pb geochronology of low-grade mafic rocks from the St. Cyr klippe and a marble from the footwall, Canadian Cordillera, Yukon

Isard, S.J., Gilotti, J.A., McClelland, W.C., Petrie, M.B., and van Staal, C.R., 2016. Geology and U-Pb geochronology of low-grade mafic rocks from the St. Cyr klippe and a marble from the footwall, Canadian Cordillera, Yukon; Geological Survey of Canada, Current Research 2016-1, 22 p. doi:10.4095/297474

Abstract: A series of thin thrust slices form a klippe in the northwest part of the St. Cyr area, west of the South Canol Road, in south-central Yukon. The uppermost unit of the klippe, the Tower Peak unit, overlies a mafic-ultramafic unit, which in turn sits on a footwall of phyllite, marble, and limestone. The Tower Peak unit is a metabasalt the trace-element geochemistry of which suggests an oceanic or island-arc origin. The U-Pb ion microprobe ages of zircon from three samples of the Tower Peak unit define a xenocrystic zircon population with abundant Precambrian and lesser Paleozoic and Mesozoic magmatic components. Jurassic grains are euhedral, oscillatory zoned, and high-temperature, with Th/U ratios approximately 0.4, and positive Ce and negative Eu anomalies, pointing to an igneous origin. A similar population of five Mesozoic zircon crystals was found in a gabbro east of the Canol Road. All of the zircon crystals are interpreted as xenocrysts entrained in the mafic magmas during emplacement due to the large age spread and lack of a consistent magmatic age. The oldest possible intrusive age for the Tower Peak unit is Upper Jurassic, and Lower Cretaceous for the gabbro to the southeast. Detrital zircon samples from a prominent marble in the footwall of the klippe define a maximum depositional age of 368 ± 6 Ma. The marble likely correlates with the Finlayson assemblage of the Yukon-Tanana terrane composite arc. The mafic-ultramafic rocks at Tower Peak were structurally amalgamated with Mesozoic rocks during formation of the St. Cyr klippe.

Résumé : Une série de minces lambeaux de charriage forment une klippe dans la partie nord-ouest de la région de St. Cyr, à l'ouest de la route Canol Sud, dans le centre sud du Yukon. L'unité sommitale de la klippe, l'unité de Tower Peak, surmonte une unité mafique-ultramafique qui, à son tour, repose sur un mur de phyllade, de marbre et de calcaire. L'unité de Tower Peak est un métabasalte dont la géochimie des éléments traces laisse croire à une origine en milieu océanique ou d'arc insulaire. Les âges U-Pb sur zircon obtenus par analyse à la microsonde ionique de trois échantillons de l'unité de Tower Peak définissent une population de xénocristaux de zircon renfermant en abondance des composantes magmatiques du Précambrien et, en moindres quantités, du Paléozoïque et du Mésozoïque. Les grains jurassiques sont idiomorphes, à zonation oscillatoire et formés à haute température, avec des rapports Th/U d'environ 0,4 et des anomalies positives en Ce et négatives en Eu, ce qui laisse croire à une origine ignée. Une population similaire de cinq cristaux de zircon du Mésozoïque a été relevée dans un gabbro à l'est de la route Canol. Selon notre interprétation, tous les cristaux de zircon seraient des xénocristaux entraînés dans les magmas mafiques lors de leur mise en place en raison de la large plage d'âges et de l'absence d'un âge magmatique cohérent. Le plus ancien âge intrusif possible pour l'unité de Tower Peak se situe au Jurassique supérieur, alors que pour le gabbro au sud-est, il correspond au Crétacé inférieur. Les zircons détritiques d'une unité saillante de marbre dans le mur de la klippe définissent un âge de sédimentation maximal de 368 ± 6 Ma. Le marbre peut vraisemblablement être corrélé à l'assemblage de Finlayson de l'arc composite du terrane de Yukon-Tanana. Les roches mafiques-ultramafiques au pic Tower ont été tectoniquement unies à des roches du Mésozoïque lors de la formation de la klippe de St. Cyr.

INTRODUCTION

The northern Cordillera is a complex orogen built of numerous terranes with continental, arc or oceanic affinities that were eventually accreted to North America in the Mesozoic (Wheeler et al., 1991; Monger and Price, 2002; Colpron et al., 2007; Nelson et al., 2013). Mafic-ultramafic rock associations occur sporadically throughout the northern Cordillera, and their terrane affinity can be difficult to assess. This is particularly problematic in Yukon, where mafic-ultramafic complexes are intercalated with the Yukon-Tanana terrane (Colpron, 2006)—a large, composite arc built on a Neoproterozoic to earliest Devonian, sedimentary substrate that was rifted from Laurentia (Fig. 1) in the Devonian. The mafic-ultramafic complexes are commonly attributed to the Slide Mountain terrane, which is generally interpreted to have evolved as a back-arc basin between the Yukon-Tanana terrane and North America and developed into an ocean of unknown dimensions synchronously with arc magmatism in the Yukon-Tanana terrane (Murphy et al., 2006; Colpron et al., 2007); however, many of the mafic-ultramafic complexes attributed to the Slide Mountain terrane may be part of other cryptic oceanic or back-arc basins, or oceanic arcs that were derived from the west and emplaced into Yukon-Tanana terrane rocks during Mesozoic accretion.

The Geological Survey of Canada initiated a study of mafic-ultramafic complexes in the intermontane terranes of the Canadian Cordillera as part of the Geo-mapping for Energy and Minerals (GEM) program. This project aims to better characterize the geochemistry and geochronology of the mafic-ultramafic complexes in order to improve models for terrane accretion in the northern Cordillera. Resolving the timing and style of terrane accretion and modification in the Canadian Cordillera is critical to better understanding the distribution of mineral resources.

The St. Cyr area in south-central Yukon (Fig. 2) is an example of a place where mafic-ultramafic rocks are intercalated with parts of the Yukon-Tanana terrane. The area is a 70 km long by 15 km wide, northwest-striking metamorphic complex that lies between the Tintina and Teslin dextral strike-slip faults between 61°22′N and 61°N (Fig. 1). Much of the area was originally mapped as the Anvil allochthon and thought to be an ophiolite associated with the Anvil Ocean (Tempelman-Kluit, 1979, 2012). Tempelman-Kluit (1979, 2012) described units in the St. Cyr area as greenschist- to amphibolite-facies metabasalt surrounded by large serpentinite lenses related to the Anvil Ocean. These mafic-ultramafic complexes, along with associated chert and deep-water sedimentary rocks in other areas, were later assigned to the Slide Mountain terrane (Wheeler et al., 1991; Colpron, 2006). Recent mapping of the St. Cyr area

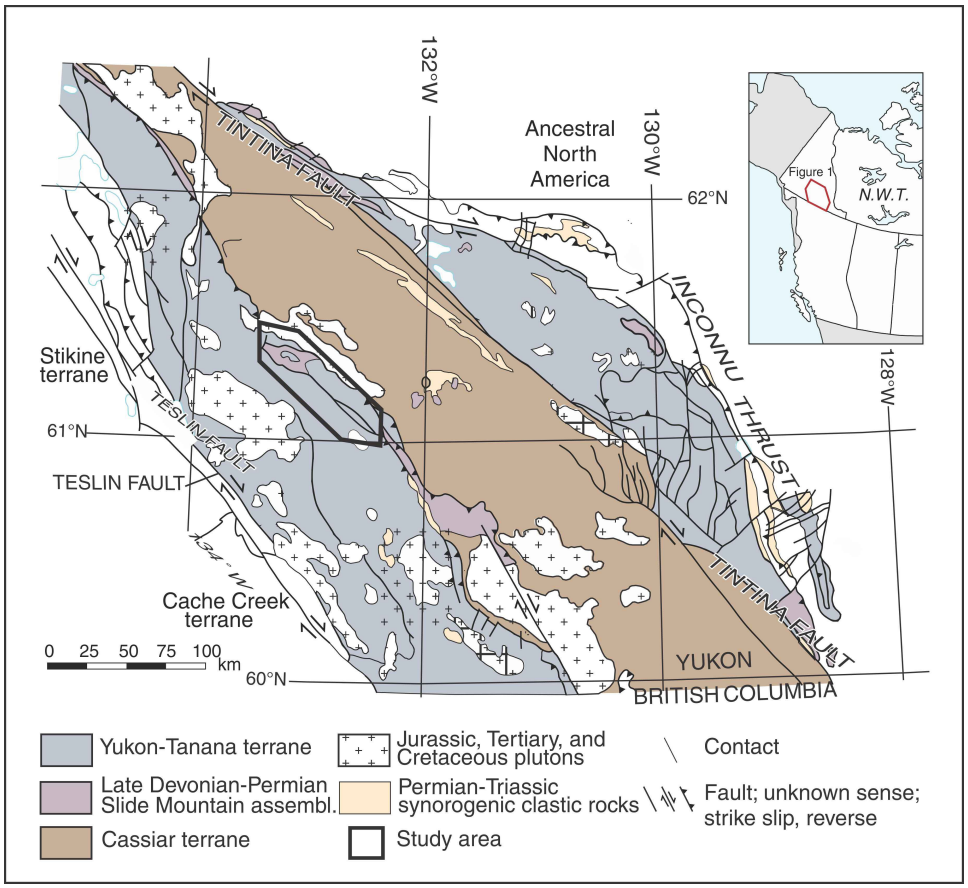

Figure 1. Simplified map of southeastern Yukon (*modified from* Colpron et al., 2006). St. Cyr study area is marked by the thick black line. assembl. = assemblage

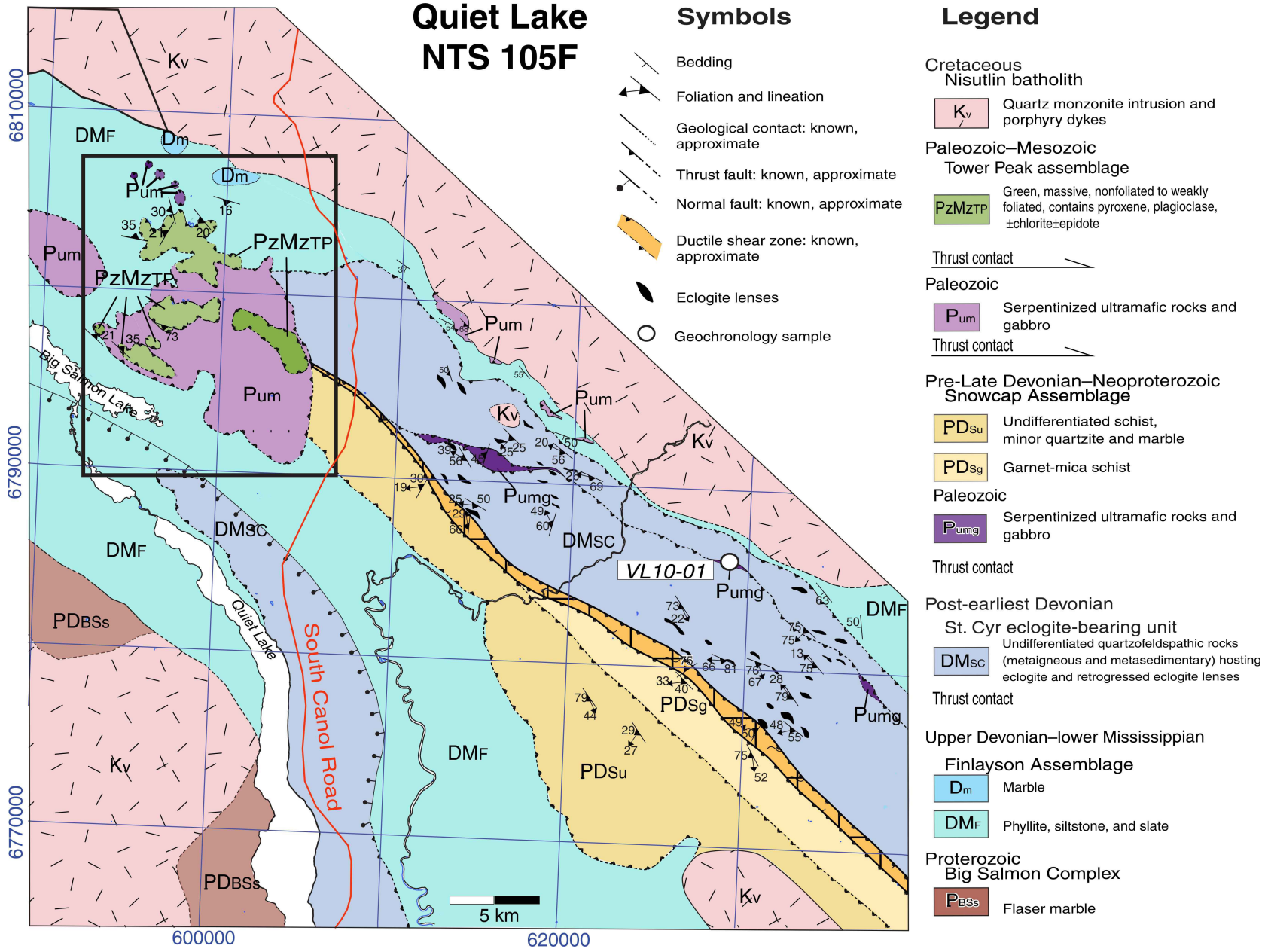

Figure 2. Geological map of the St. Cyr area based on mapping by Isard (2014), Petrie et al. (2015), the Quiet Lake (105F) map of Tempelman-Kluit (2012), and the regional map of Colpron (2006). Darker shades indicate areas of extensive outcrop exposure. Box marks the outline of Figure 3.

(Petrie et al., 2015) has shown that there is less mafic-ultramafic material than shown on previous maps. In particular, metre- to hundreds of metre-long lenses of eclogitic rocks are hosted by quartzofeldspathic schist units that have igneous and sedimentary protoliths, and belong to the Yukon-Tanana composite arc (Gilotti et al., 2013; Petrie et al., 2015). These form coherent slices of continental arc crust up to 30 km long.

This study focuses on a small part of the St. Cyr area, west of the South Canol Road (Fig. 2), where a mafic-ultramafic unit and a metabasalt (Tower Peak unit) are found in the hanging wall of a klippe. The Tower Peak unit was described by Fallas et al. (1999) as a greenschist-facies metavolcanic complex, but the unit has few age or geochemical constraints. This study explores the age and tectonic setting of the Tower Peak unit. Geochemistry of four samples indicates that the protolith of the Tower Peak unit was an oceanic or island-arc basalt. Sensitive high-resolution ion microprobe-reverse geometry (SHRIMP-RG) U-Pb zircon geochronology reveals that the Tower Peak unit may be at least Jurassic. A gabbro intercalated with the eclogite-bearing slices that lies east of the South Canol Road also contains Mesozoic zircon grains, and is included in this report. A Mesozoic age negates any link to the Paleozoic Slide Mountain Ocean. The present authors also determined the age of a metasedimentary rock in the footwall of the St. Cyr klippe using detrital zircon from a marble in the northwestern part of the study area. The maximum depositional age is consistent with the footwall of the klippe being part of the earliest arc (Finlayson) assemblage of the Yukon-Tanana terrane.

REGIONAL GEOLOGY

The Yukon-Tanana terrane is one of several composite arcs, together with Stikinia and Quesnellia, formed on a substrate of Laurentian crust that is interpreted to have rifted away from Laurentia in the Devonian (Nelson et al., 2013 and references therein). These terranes were separated from Laurentia by the Slide Mountain terrane, which formed the intervening oceanic regime between the arcs and Ancestral North America (Fig. 1; Monger et al., 1982; Wheeler et al., 1991; Colpron et al., 2006, 2007). All of these terranes can be considered part of the Peri-Laurentian realm (Colpron et al., 2006, 2007; Nelson et al., 2006, 2013), as their ties to Laurentia are well established. The Peri-Laurentian terranes along with the outboard oceanic and accretionary complex of the Cache Creek terrane were accreted to Laurentia in the Early to Middle Jurassic (Monger and Price, 2002; Nelson et al., 2013) and then further imbricated during interaction and accretion with outboard arc terranes of the Insular belt (Alexander and Wrangellia terranes) that comprise the westernmost parts of the Northern Cordillera (McClelland and Gehrels, 1990; van der Heyden, 1992). The Whitehorse trough records Upper Triassic to Middle Jurassic sedimentation in a forearc basin that evolved into a collisional basin; sediments were sourced in the rapidly exhuming terranes that surround the area such as the Yukon-Tanana terrane, Stikinia, Quesnellia, and related plutons (Colpron et al., 2015). In south-central Yukon (Fig. 1), the Yukon-Tanana terrane is dismembered by two major strike-slip fault systems, the Teslin and Tintina, active in the Eocene (Gabrielse et al., 2006). These faults cut the Cretaceous to Jurassic thrusts that emplaced Yukon-Tanana terrane onto Ancestral North America.

The Slide Mountain terrane is an oceanic assemblage consisting of discontinuous slivers of low-grade mafic and ultramafic rocks and associated pelagic sedimentary rocks that stretches from southern British Columbia to northern Yukon (Nelson et al., 2013, and references therein). The Slide Mountain terrane has a long-lived history from Late Devonian to Late Triassic (Wheeler et al., 1991; Mortensen, 1992a). The mafic-ultramafic rocks commonly include metabasalt, gabbro, harzburgite, and serpentinite that are locally strongly tectonized. Some areas, such as the Sylvester allochthon (Nelson, 1993), the Anvil district (Pigage, 2004), and the Finlayson Lake massive-sulphide district (Murphy et al., 2006), contain thick packages of marine chert and argillite. Carboniferous to Permian conodonts, fusulinids and radiolarians provide some age constraints on the stratigraphic units (Nelson and Bradford, 1993; Pigage, 2004; Orchard, 2006). Uranium-lead zircon dates, mostly from gabbro samples assigned to the Slide Mountain terrane, give similar Carboniferous to Permian ages (e.g. Mortensen, 1992a; Murphy et al., 2006; Colpron et al., 2006). The Slide Mountain Ocean closed during the Permian to the Triassic (Mortensen, 1992b; Nelson et al., 2006; Beranek and Mortensen, 2011).

GEOLOGY OF THE NORTHWEST ST. CYR KLIPPE

The St. Cyr klippe is located approximately 15 km northeast of Quiet Lake, Yukon within the Quiet Lake 1:250 000 map sheet (NTS 105F; Tempelman-Kluit, 1979, 2012). Slices of Yukon-Tanana terrane rocks contain Permian eclogite in the southeast part of the area (Erdmer, 1992; Petrie et al., 2015). This study focuses on the structurally highest, noneclogite-bearing units of the St. Cyr klippe west of the South Canol Road (Fig. 2, 3) and is the subject of a recent M.Sc. thesis (Isard, 2014). Here the authors describe the three main units from the structurally highest to lowest: the Tower Peak unit, a mafic-ultramafic unit, and metasedimentary rocks in the footwall of the klippe. The units are separated by low-angle thrust faults with varying degrees of associated brittle deformation.

Tower Peak unit

Lithology

The Tower Peak unit (Fallas et al., 1999) is a massive to weakly foliated, grey to green, very fine- to medium-grained mafic rock (Fig. 4a) that occupies the top of the St. Cyr klippe. The unit is devoid of features such as dykes, pillows, or flows that would help to interpret its origin. The unit also has a strong brittle overprint and is commonly cut by secondary quartz and calcite veins (Fig. 4b). Adjacent to the fault zones, the rocks are brecciated and locally they are cataclasite and ultracataclasite.

The mineralogy of these fine-grained rocks was determined with the aid of energy-dispersive spectrometry using the Hitachi S3400 scanning electron microscope (SEM), University of Iowa, Iowa City, Iowa. The rocks are mainly composed of plagioclase and clinopyroxene (Fig. 4c) with an interlocking, subophitic texture suggestive of a diabase. The rocks typically have a very fine-grained, felted

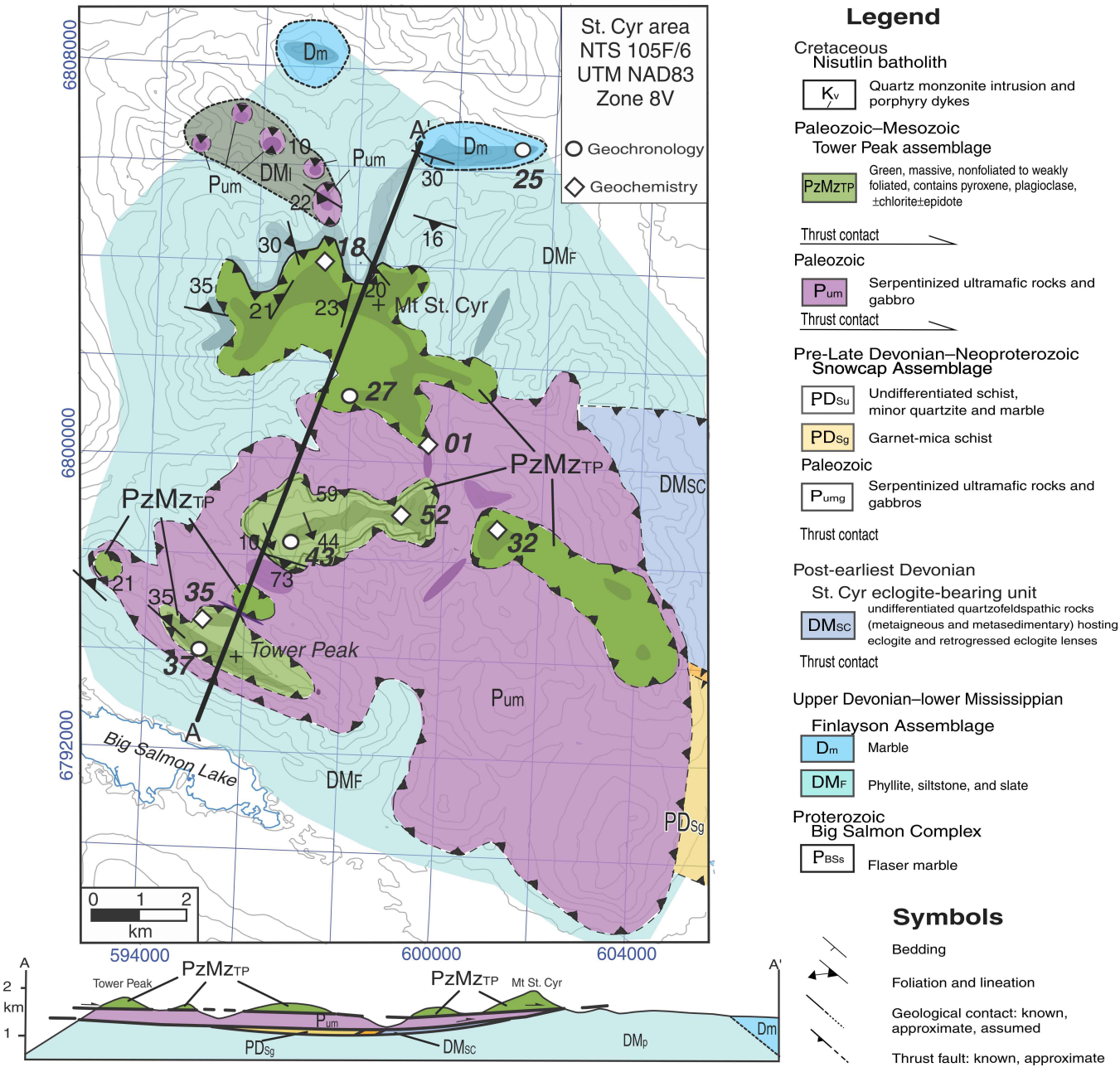

Figure 3. Geological map of the northwest St. Cyr area (west of the South Canol Road) showing sample locations and cross-section A-A′ (V = H). Darker shades indicate areas of extensive outcrop exposure; DMl = Devonian-Mississippian limestone, DMp = Devonian-Mississippian phyllite. Unit boxes with no colour do not appear on this map.

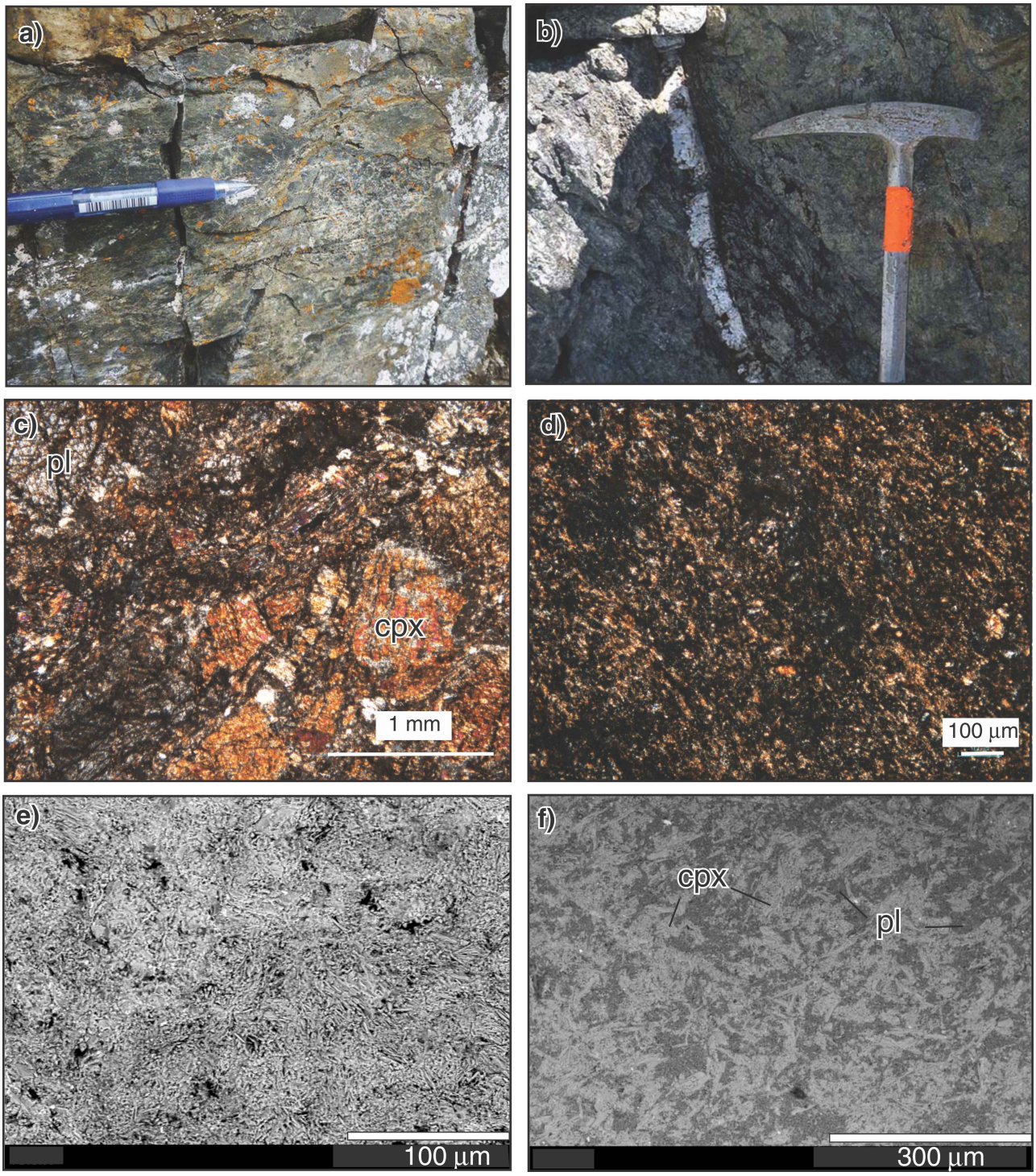

Figure 4. Tower Peak unit: **a)** photograph of a representative outcrop of fine-grained, massive metabasalt; the length of the pen shown is approximately 10 cm; photograph by S.J. Isard; 2016-033; **b)** typical quartz vein cuts the metabasalt; length of the hammer head is approximately 20 cm; photograph by S.J. Isard; 2016-034; **c)** photomicrograph showing fractured grains of plagioclase (pl) and clinopyroxene (cpx), in sample 13-52, crosspolarized light; photograph by S.J. Isard; 2016-031; **d)** photomicrograph of the fine-grained matrix in sample 13-01, crosspolarized light; photograph by S.J. Isard; 2016-029; **e)** back-scattered electron image of sample 13-52, showing the a matted texture of the fine-grained matrix with pyroxene (bright) and plagioclase blades; 2016-023; **f)** back-scattered electron image of sample 13-01 shows that plagioclase (pl) and pyroxene (cpx) are the main phases; 2016-027

groundmass (Fig. 4d, e, f) consisting mainly of plagioclase and clinopyroxene. The igneous assemblage is overprinted by greenschist-facies minerals including epidote, chlorite, and titanite. Quartz and calcite veins likely derive from secondary fluids associated with the brittle deformation.

Geochemistry

Major- and trace-element geochemistry are presented for four Tower Peak samples (Table 1) in order to characterize the possible protolith. Samples were analyzed at the GeoAnalytical Laboratory of Washington State University, Pullman, Washington. Major elements were collected using X-Ray Fluorescence on a ThermoARL Advant'XP+ automated sequential wavelength spectrometer, and are reported as oxide minerals. Trace elements were collected with an Agilent 7700 inductively coupled plasma mass spectrometer (ICP-MS).

Because the Tower Peak unit has undergone greenschist-facies metamorphism, most major elements and low-field-strength elements (LFSE) have likely experienced mobilization, and are therefore not reliable for discrimination between rock types (MacLean, 1990). Immobile elements such as high-field-strength elements (HFSEs), rare-earth elements (REEs), and Th are more reliable discriminates (Pearce and Cann, 1973; MacLean, 1990). The SiO_2 content ranges from 45–58 weight per cent, and all four samples plot within the basalt field in Zr/TiO_2 versus Nb/Y space (Fig. 5a). The samples demonstrate enrichment in large-ion lithophile elements (LILEs) as well as relatively constant heavy rare-earth elements (HREEs; Fig. 5b). Samples 13-01 and 13-32 show flat REE signatures. Sample 13-35 has enriched LREEs with constant HREEs, whereas sample 13-52 is depleted in all elements compared to the other samples, but has a similar pattern to that of sample 13-35.

A Zr-Th-Nb ternary plot (Wood, 1980; Fig. 5c) aids in determining the tectonic environment in which the Tower Peak unit formed, and a Th-Nb diagram (Pearce, 2008; Fig. 5d) assists in determining whether a sample underwent significant crustal contamination. Samples 13-01 and 13-32 plot within the N-MORB field, and marginally above the MORB array in the Th-Nb diagram indicating little, if any crustal contamination or subduction component. The other two samples fall in the arc-basalt field in the ternary plot. These samples plot above the MORB-OIB array in the Th-Nb plot, indicating crustal assimilation or a subduction component (Pearce, 2008). This is further illustrated in sample 13-52 by the Nb anomaly seen in Figure 5b and the Th/Nb ratios greater than 0.2, which are typical of continental crust and arc basalt.

Mafic-ultramafic unit

The mafic-ultramafic unit lying beneath the Tower Peak metabasalt is a strongly deformed, imbricated package of low-grade metagabbro with rare amphibolite, pyroxenite, and serpentinite. The gabbro is black, fine- to coarse-grained, and massive to foliated. A rare 1–2 m thick, massive, coarse-grained amphibolite (metagabbro) lens was found at one locality. The gabbro units are cut by calcite veins (Fig. 6a) that are probably related to brittle deformation during thrusting. Orange-weathering, massive ultramafic rocks are found as lenses surrounded by serpentinite. Some of the pyroxenite contains oxide pseudomorphs after chromite. The ultramafic lenses can be up to tens of metres thick, and they are all variably serpentinized. The serpentinite is green to black, massive to fibrous lizardite (Fig. 6b) (Isard, 2014). The presence of lizardite indicates that the serpentinite formed at temperatures below 300°C (Evans et al., 2013). Serpentinite contacts have the potential to host nephritic jade, such as that found in the King Arctic mine in the southern Campbell Range to the east (Fig. 1; Devine et al., 2004), but systematic mapping did not identify any large jade deposits (Isard and Gilotti, 2014).

Footwall units

The footwall of the St. Cyr klippe is assigned to the Devonian to Mississippian Finlayson assemblage of the Yukon-Tanana terrane on regional maps (Colpron, 2006), but there is very little age control in the Quiet Lake map area. In the northwest St. Cyr area (Fig. 3), the footwall is made up of phyllite, marble, and limestone. Black to dark green phyllite, consisting of quartz+biotite±chlorite and secondary calcite (Fig. 7a, b), is the dominant lithology. The phyllitic cleavage is defined by the preferred orientation of biotite seams that anastomose around single quartz grains and polycrystalline quartz-rich domains (Fig. 7a). The polycrystalline quartz is the result of low-temperature, bulging recrystallization (e.g. Stipp et al., 2002). The phyllitic cleavage is folded in some small areas, creating a weak crenulation cleavage, and generally dips gently to the southwest or northeast.

An approximately 100 m thick marble unit (Fig. 7c, d) is exposed in the northern part of the map area (Fig. 3). The marble is coarse grained with approximately 0.5–5 cm thick, alternating dark and light grey layers that dip 30° southwest. This unit overlies the phyllite units, with a sharp contact dipping approximately 45° to the east (Fig. 7d). The contact between the phyllite and the marble may be primary, in which case the layering in the marble and the phyllitic cleavage are at a high angle to original layering, or more likely the contact is a fault. In the northwest part of the study area, a medium-grained limestone outcrops with resistant, 1–3 cm thick quartz veins. Templeman-Kluit (2012) suggested that the limestone was metamorphosed to form marble in the contact aureole of the Nisutlin batholith, but the present authors were unable to evaluate this possibility.

Table 1. Tower Peak major- and trace-element geochemistry.

Sample ID	13-01	13-32	13-35	13-52
UTM Location	*Zone 8V*			
E (m)	0599107	0600870	0595689	0599424
N (m)	6802484	6798579	6797091	6799340
SiO_2 (wt%)	49.14	42.57	54.68	53.35
TiO_2	1.583	0.417	0.657	0.116
Al_2O_3	15.02	16.65	16.81	1.93
FeO*	10.46	5.73	8.18	5.13
MnO	0.189	0.128	0.145	0.113
MgO	7.00	12.41	5.38	18.56
CaO	10.26	15.66	2.11	18.07
Na_2O	3.24	0.58	4.97	0.12
K_2O	0.29	0.05	0.96	0.00
P_2O_5	0.153	0.032	0.185	0.005
Sum	97.35	94.22	94.07	97.40
LOI (%)	2.11	5.49	5.35	1.52
La (ppm)	4.15	1.10	9.53	0.71
Ce	12.77	2.73	20.50	0.91
Pr	2.19	0.47	2.92	0.13
Nd	11.59	2.56	12.71	0.59
Sm	4.15	1.02	3.04	0.23
Eu	1.42	0.53	1.05	0.11
Gd	5.49	1.46	3.00	0.39
Tb	1.04	0.28	0.48	0.07
Dy	6.93	1.88	2.94	0.55
Ho	1.49	0.41	0.62	0.12
Er	4.12	1.12	1.71	0.32
Tm	0.61	0.16	0.25	0.05
Yb	3.72	0.99	1.56	0.28
Lu	0.59	0.16	0.25	0.04
Ba	82	39	714	13
Th	0.24	0.06	1.47	0.02
Nb	2.16	0.58	4.21	0.03
Y	37.45	10.16	15.36	2.90
Hf	3.06	0.58	2.04	0.06
Ta	0.17	0.04	0.20	0.00
U	0.18	0.02	0.56	0.01
Pb	0.58	0.14	1.72	0.40
Rb	5.8	0.8	17.6	0.2
Cs	0.22	0.13	0.73	0.04
Sr	129	47	98	7
Sc	39.0	30.8	28.6	64.1
Zr	114	19	73	2
Th/Nb	0.111	0.103	0.349	0.667
Th/Yb	0.065	0.061	0.942	0.071
Nb/Yb	0.581	0.586	2.699	0.107
Nb/16	0.135	0.036	0.263	0.002
Zr/117	0.974	0.162	0.624	0.017

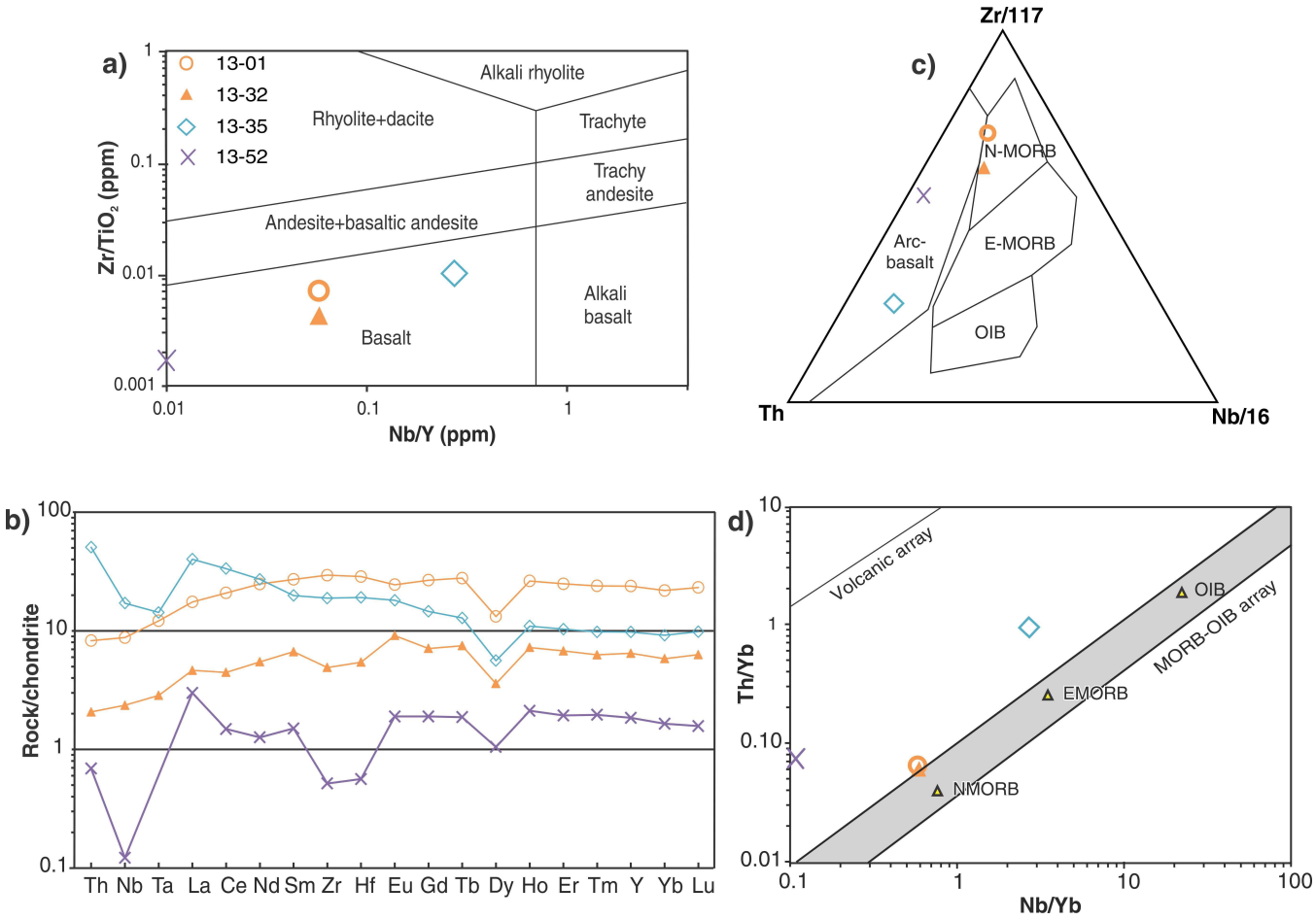

Figure 5. Geochemistry of the Tower Peak unit: **a)** Zr/TiO_2 versus Nb/Y discrimination diagram (*after* Winchester and Floyd, 1977 *modified from* Pearce, 1996). All samples plot within the basalt field; **b)** extended REE plot normalized to chondritic values (*after* Sun and McDonough, 1989); **c)** Th-Zr-Nb ternary plot (*after* Wood, 1980). Samples 13-01 and 13-32 plot within the N-MORB field, whereas the other two samples plot within the arc-basalt field; **d)** a Th-Nb plot (*after* Pearce, 2008). Samples 13-01 and 13-32 plot on the transition from MORB to OIB, whereas the other two samples indicate crustal contamination or a subduction component.

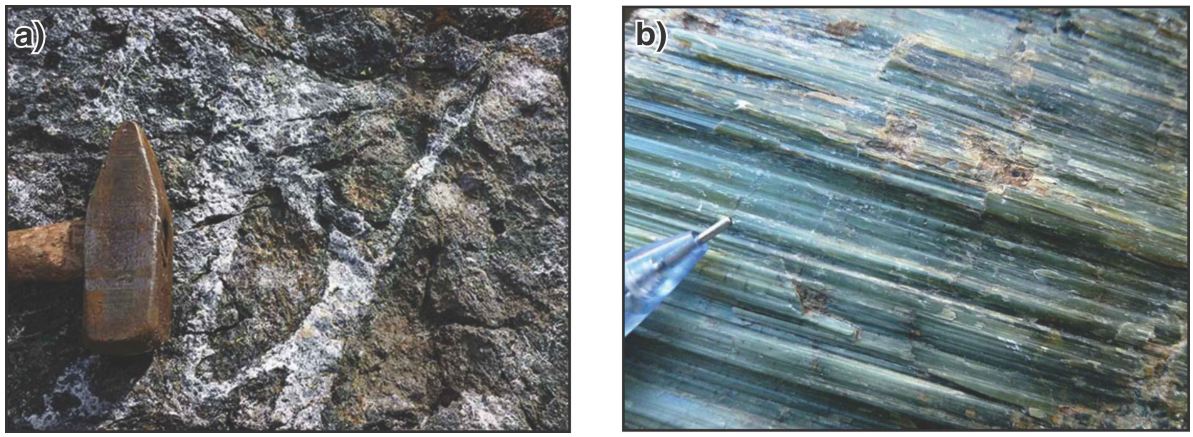

Figure 6. Mafic-ultramafic unit: **a)** calcite veins in a massive gabbro; hammer head is approximately 15 cm long; 2016-028; and **b)** fibrous serpentinite; pen tip is 1 cm; 2016-026; photographs by S.J. Isard.

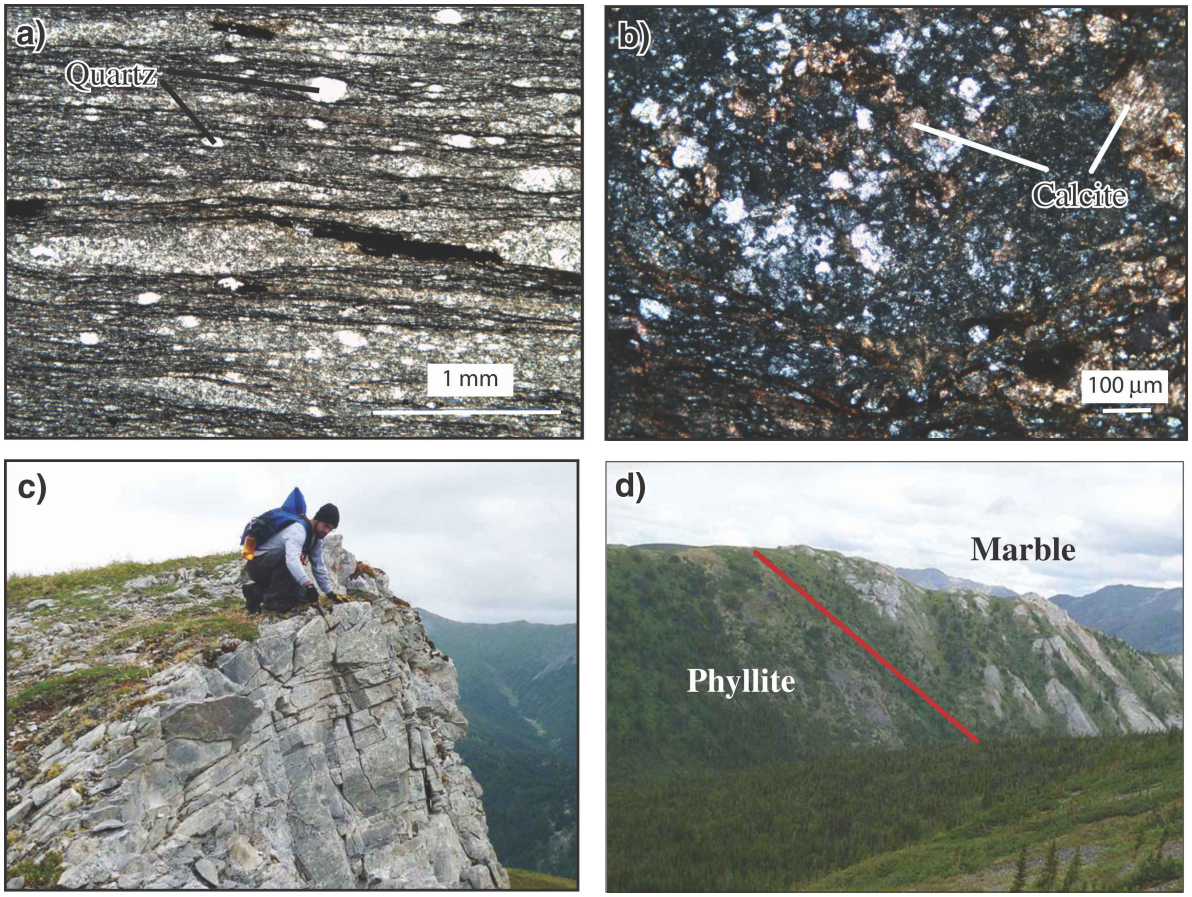

Figure 7. Footwall units: **a)** photomicrograph of quartz-rich microlithons and biotite-rich cleavage seams in phyllite. Sample 13-10, plane-polarized light; 2016-032; **b)** secondary calcite in the phyllite, sample 13-10, crosspolarized light; 2016-030; **c)** marble with field assistant (person squatting is 1 m) for scale; 2016-025; **d)** contact between phyllite and marble (red line) looking north; there are trees in the foreground; trees on the marble may be 2–3 m tall; 2016-024; photographs by S.J. Isard.

STRUCTURAL GEOLOGY

The geological map in Figure 3 is the result of three weeks of fieldwork by Isard in July–August, 2013. Mountains and ridges above tree line are well exposed, but areas in the valleys are heavily covered. The highest peaks are made up of the Tower Peak unit, which is well exposed at Mount St. Cyr in the north and Tower Peak in the south. The Tower Peak unit sits above a mixture of mafic and ultramafic rocks (mapped as one unit) on a subhorizontal fault, and thus forms a klippe. This relationship is best seen in the southwestern portion of the mapping area where a several metre wide trough of serpentinite separates two summits of the Tower Peak unit at Tower Peak. This fault contact is weakly brecciated. In most of the area, the mafic-ultramafic unit structurally overlies the marble and phyllite units of the footwall above another shallowly dipping fault. This is best seen in the northwestern part of the study area where small gabbroic klippen sit above limestone on a sharp fault contact with little or no cataclasis. In the vicinity of Mount St. Cyr, the mafic-ultramafic unit is excised, and the Tower Peak unit rests directly on the phyllite; the contact is brecciated in a zone up to 10 m thick and locally contains fault gouge.

No kinematic information was obtained from the fault rocks, but the faults are assumed to be northeast-directed thrusts based on comparison with regional structures documented to the north (Fig. 1, Colpron et al., 2005). Thrusting took place in the brittle regime, and postdates the greenschist-facies fabrics in the phyllite. Erosion of the thin, subhorizontal thrust sheets of the Tower Peak and mafic-ultramafic units forms a composite klippe that rests above phyllite and marble in the footwall. These relationships are illustrated in the cross-section in Figure 3. The Cretaceous Nisutlin batholith (Fig. 2; Tempelman-Kluit 1979, 2012) crosscuts units of the footwall, the mafic-ultramafic unit, and the Tower Peak unit and limits the time of the thrusting to a preintrusion age.

To the southeast (Fig. 2), an imbricate stack of thrust sheets underlies the klippe described above. These imbricates consist of high-grade, eclogite- and noneclogite-bearing

units of the Yukon-Tanana terrane that are intercalated with slices of mafic and ultramafic rocks (Petrie et al., 2015). The relationship among the different mafic-ultramafic units is unclear, but is the subject of additional studies (C.R. van Staal, work in progress, 2016). The difference in structural style (imbricates versus klippen), deformation regime (ductile versus brittle), metamorphic grade (eclogite- and amphibolite facies versus greenschist facies) east and west of the South Canol Road suggests there was no prior relationship between the imbricate slices to the southeast and the units located in the northwest. The younger-on-older and low-grade on high-grade relationship between the Tower Peak and mafic-ultramafic units and the underlying St. Cyr imbricated rocks suggests that the bounding fault is a pre-Nisutlin batholith, out-of-sequence thrust.

URANIUM-LEAD ZIRCON GEOCHRONOLOGY OF THE TOWER PEAK UNIT AND A GABBRO

A limited amount of zircon was separated from three representative samples (13-27, 13-37, 13-43) of fine-grained metabasalt from the Tower Peak unit (Fig. 3) and one gabbro (VL10-01) from the St. Cyr area (Fig. 2). The gabbro, collected by C.R. van Staal, is included here because it too contains an unexpected population of young grains. The sample is from a horse of serpentinized ultramafic rocks and gabbro that sits in a thrust zone between slices of eclogite-bearing arc crust (Petrie et al., 2015). The gabbro is a deformed, L>S tectonite that is enclosed by amphibolitic gabbro along with harzburgite and dunite. All the recovered zircon grains were subsequently imaged and analyzed.

Analytical methods

The samples underwent standard crushing, and heavy liquid- and magnetic separation before zircon grains were handpicked under alcohol. Zircon grains were mounted in epoxy resin with natural zircon standards before being polished to expose grain centres. The zircon grains were imagined by cathodoluminescence on the JEOL SEM at the Stanford–U.S. Geological Survey Micro Analysis Center, Stanford, California (Fig. 8). Zircon was analyzed on the sensitive high-resolution ion microprobe-reverse geometry (SHRIMP-RG) following procedures outlined by Barth and Wooden (2006) for U-Pb geochronology and Mazdab and Wooden (2006) for trace-element geochemistry. Trace-element and U-Th-Pb data were collected simultaneously.

Natural zircon standard R33 (421 Ma; Black et al., 2004; Mattinson, 2010) was used to correct for isotopic compositions and fractionation through replicate analysis. Uranium concentrations were standardized against Madagascar Green (MADDER)—a well characterized, homogeneous, in-house zircon standard that is calibrated relative to MAD-green (4196 ppm U, Barth and Wooden, 2010). The analytical session for the Tower Peak samples had a 2σ calibration error for R33 with a $^{206}Pb/^{238}U$ ratio of 0.46%. The trace-element routine collected ^{139}La, ^{140}Ce, ^{146}Nd, ^{147}Sm, ^{153}Eu, $^{157}Gd^{16}O$, $^{163}Dy^{16}O$, $^{166}Er^{16}O$, $^{172}Yb^{16}O$, ^{180}Hf, ^{16}O, ^{48}Ti, and ^{49}Ti, with concentrations calibrated against zircon standards MADDER (Mazdab and Wooden, 2006). Gabbro VL10-01 was run in a separate session and had a 2σ calibration error for the R33 $^{206}Pb/^{238}U$ ratio of 0.66%. An abbreviated trace-element routine analyzed ^{139}La, ^{140}Ce, ^{146}Nd, ^{147}Sm, ^{153}Eu, ^{155}Gd, $^{179}Dy^{16}O$, $^{166}Er^{16}O$, $^{172}Yb^{16}O$, ^{180}Hf, and ^{16}O, using the same standard.

SHRIMP-RG U-Pb data are presented in Table 2 and trace-element data in Table 3. Titanium (^{48}Ti and ^{49}Ti) concentrations were measured for zircon from the Tower Peak unit. Ti-in-zircon crystallization temperatures were calculated using ^{49}Ti to avoid interference with the $^{96}Zr^{2+}$ peak (Watson and Harrison, 2005), and followed the method outlined by Ferry and Watson (2007). Titanium and temperature data are presented in Table 3.

Results

Tower Peak unit

Twenty-five colourless zircon grains were extracted from three samples. They range in size from 50 μm to 125 μm, in shape from rounded to euhedral, and show different levels of brightness and zoning in cathodoluminescence images (Fig. 8). The zircon grains fall into three different age populations—Proterozoic, Paleozoic, and Mesozoic.

The majority of zircon grains are Proterozoic with $^{206}Pb/^{238}U$ ages as young as 650 Ma and $^{207}Pb/^{206}Pb$ ages as old as 2660 Ma (Fig. 9a). These grains have a rounded morphology and are cathodoluminescence-dark. Many have distinct, euhedral cores with faint oscillatory zoning. All of the grains are characterized by a positive Ce anomaly, a negative Eu anomaly, steep HREE pattern (Yb/Gd = 4–52; Fig. 10), and Th/U ratios between 0.1 and 1.5. Ti-in-zircon temperatures range from 655°C to1153°C (Fig. 11).

Paleozoic ages are seen in four grains with ^{207}Pb-corrected $^{206}Pb/^{238}U$ ages between 303 Ma and 433 Ma (Fig. 9b). Morphology and cathodoluminescence response varies. Grain 10 in sample 13-37 is euhedral and cathodoluminescence-light grey with well developed oscillatory zoning. The grain has a thin, distinct, cathodoluminescence-dark halo that may represent a metamorphic rim. Grain 1 is euhedral, but is cathodoluminescence-dark with a dark grey euhedral core. Grain 3 is also cathodoluminescence-dark with a euhedral core, but is rounded with grain boundaries that clearly truncate internal oscillatory zoning. Grain 1 of sample 13-43 is cathodoluminescence-medium grey and homogenous. All four grains have a positive Ce anomaly, a slight negative Eu anomaly, steep HREE pattern (Yb/Gd = 4–10; Fig. 10), and Th/U ratios ranging from 0.1 to 1.4. Ti-in-zircon temperatures are 703°C to 959°C (Fig. 11).

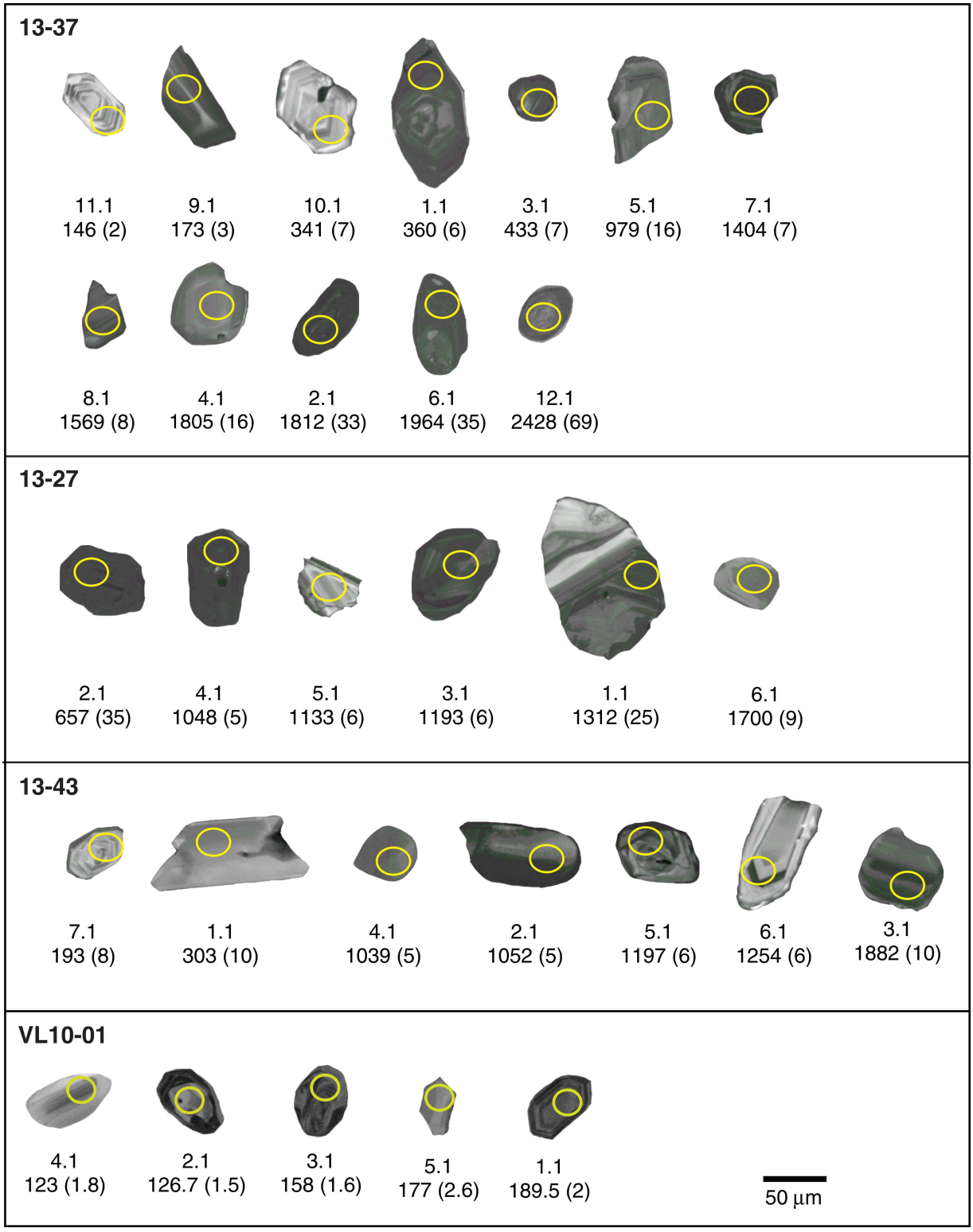

Figure 8. Cathodoluminescence images of all the zircon grains from three samples of the Tower Peak unit (13-37, 13-27, and 13-43) and a gabbro from the St. Cyr area (VL10-01) that were analyzed for U-Pb and trace elements. Ellipses indicate analysis spots. Grain (number.spot) number and age (uncertainty in million years (Ma)) shown below each zircon.

Table 2. SHRIMP U-Pb geochronological zircon data and apparent ages.

Spot	CL[a]	U (ppm)	Th (ppm)	Th/U (ppm)	$^{206}Pb^{*b}$	$f^{206}Pb_c$ [b]	$^{238}U/^{206}Pb^{c}$		$^{207}Pb/^{206}Pb^{c}$ (Ma)		$^{206}Pb/^{238}U^{d}$ (Ma)		$^{207}Pb/^{206}Pb$	
Sample 13-37 *UTM: Zone 8V E 0595591 m, N 6795941 m*														
11.1	om	467	200	0.4	9	0.98	43.318	(1.5)	0.05677	(2.7)	146	(2)		
9.1	om	710	303	0.4	17	<0.01	36.875	(1.6)	0.04914	(1.8)	173	(3)		
10.1	c	338	85	0.3	16	0.34	18.335	(1.9)	0.05608	(1.8)	341	(7)		
1.1	om	757	76	0.1	37	0.69	17.276	(1.6)	0.05936	(1.1)	360	(6)		
3.1	om	557	538	1	33	0.19	14.381	(1.7)	0.05704	(1.2)	433	(7)		
5.1	om	208	90	0.4	29	0.19	6.085	(1.7)	0.07335	(1.2)	979	(16)	987	(29)
7.1	c	1186	845	0.7	248	0.06	4.109	(0.5)	0.08952	(0.6)	1404	(7)	1400	(13)
8.1	om	199	217	1.1	46	<0.01	3.71	(0.5)	0.0949	(1.4)	1539	(8)	1516	(27)
2.1	om	282	220	0.8	79	7.16	2.86	(1.8)	0.1733	(1.6	1812	(33)	2582	(27)
4.1	c	170	165	1	47	<0.01	3.098	(0.9)	0.10939	(0.8)	1805	(16)	1780	(15)
6.1	om	302	71	0.2	92	<0.01	2.81	(1.8)	0.11992	(0.5)	1964	(35)	1955	(10)
12.1	c	121	157	1.3	48	3.05	2.12	(2.7)	0.18455	(0.6)	2428	(69)	2658	(12)
Sample 13-43 *UTM: Zone 8V E 0597024 m, N 6798459 m*														
7.1	c	852	246	0.3	22	0.02	32.913	(4.2)	0.05013	(2.8)	193	(8)		
1.1		49	66	1.4	2	<0.01	20.915	(3.4)	0.04754	(6)	303	(10)		
4.1	om	182	55	0.3	27	0.08	5.714	(0.5)	0.07457	(2.1)	1039	(5)	987	(60)
2.1	om	203	13	0.1	31	0.05	5.64	(0.5)	0.07487	(1.9)	1052	(5)	1120	(48)
5.1	om	253	161	0.7	44	0.32	4.886	(0.5)	0.08272	(1.5)	1197	(6)	1250	(33)
6.1	om	330	145	0.5	61	0.15	4.65	(0.5)	0.08369	(1.3)	1254	(6)	1294	(28)
3.1	om	149	211	1.5	43	-0.32	2.96	(0.5)	0.11237	(1.4)	1882	(10)	1837	(25)
Sample 13-27 *UTM: Zone 8V E 0597900 m, N 6801555 m*														
2.1	om	873	465	0.5	80	4.1	8.939	(5.4)	0.09515	(0.6)	657	(35)	1130	(33)
4.1	om	852	508	0.6	129	2.35	5.532	(0.5)	0.09402	(0.8)	1048	(5)	1415	(23)
5.1	om	96	95	1	16	<0.01	5.207	(0.5)	0.07682	(2.6)	1133	(6)	1040	(78)
3.1	c	321	166	0.5	56	<0.01	4.932	(0.5)	0.07742	(1.4)	1193	(6)	1131	(28)
1.1	om	285	134	0.5	55	0.22	4.421	(2)	0.08675	(0.8)	1312	(25)	1351	(16)
7.1		82	118	1.5	21	<0.01	3.454	(0.5)	0.09931	(2)	1642	(9)	1592	(42)
6.1	c	211	222	1.1	55	<0.01	3.321	(0.5)	0.10254	(1.2)	1700	(9)	1670	(23)
Sample V10-01 *UTM: Zone 8V E 0629624 m, N 6785675 m*														
4.1	c	353	255	0.75	5.9	0.28	0.0507	(4.2)	51.32	(1.5)	123.3	1.8	51.65	(1.4)
2.1	c	563	424	0.78	9.6	-0.15	0.0474	(3.3)	50.66	(1.2)	126.7	1.5	50.46	(1.2)
3.1	c	752	328	0.45	16.1	0.18	0.0507	(2.4)	40.11	(1.0)	158.5	1.6	40.09	(1.0)
5.1	c	254	165	0.67	6.1	0.36	0.0525	(4.2)	36.03	(1.5)	177.0	2.6	35.80	(1.5)
1.1	c	290	139	0.49	7.4	-0.12	0.0489	(2.5)	33.58	(1.0)	189.5	2.0	33.57	(1.0)

Note: All analyses were performed on the SHRIMP-RG ion microprobe at the United States Geological Survey-Stanford Microanalytical Center at Stanford University. The analytical routine followed Barth and Wooden (2006). Data reduction utilized the SQUID 2.5 program of Ludwig (2009).

[a]Abbreviations: CL (cathodoluminescence) designations: c = core, om = oscillatory zoned mantle.

[b]Pb* denotes radiogenic Pb; Pb_c denotes common Pb; $f^{206}Pb_c = 100*(^{206}Pb_c/^{206}Pb_{total})$.

[c]Calibration concentrations and isotopic compositions were based on replicate analyses of R33 (421 Ma, Black et al., 2004; Mattinson, 2010) and Madagascar Green (MADDER; 4196 ppm U, Barth and Wooden, 2010). Reported ratios are not corrected for common Pb. Errors are reported in parentheses as percent at the 1σ level.

[d]Ages were calculated from $^{206}Pb/^{238}U$ ratios corrected for common Pb using the ^{207}Pb method and $^{207}Pb/^{206}Pb$ ratios corrected for common Pb using the ^{204}Pb method (*see* Williams, 1998). Initial common Pb isotopic composition approximated from Stacey and Kramers (1975). Uncertainties in millions of years reported as 1σ.

Table 3. Zircon trace-element data.

Spot	CL[a]	Y	La	Ce	Nd	Sm	Eu	Gd	Dy	Er	Yb	Hf	Ce/Ce*	Eu/Eu*	$Yb_{(N)}/Gd_{(N)}$	Fe	48Ti	49Ti	T (°C)
Sample 13-37																			
11.1	om	835	1.45	31	0.5	1.3	0.90	15	67	141	317	8410	20	0.6	26	68	5.2	5.1	752
9.1	om	2239	0.10	13	3.6	7.6	0.93	58	224	377	613	9388	12	0.1	13	20	13.5	13.4	850
10.1	c	650	0.01	6	0.2	0.8	0.33	10	48	122	314	8751	85	0.4	41	6	3.0	2.8	703
1.1	om	2061	2.85	20	7.4	10.5	4.33	60	236	323	522	9851	2	0.5	11	130	32.0	31.7	959
3.1	om	1617	0.07	67	2.9	6.1	0.91	48	158	269	468	9664	82	0.2	12	1	14.2	14.0	857
5.1	om	1049	0.04	26	2.0	4.1	0.34	35	113	179	291	9379	47	0.09	10	17	8.3	7.9	798
7.1	c	5679	8.97	121	18.3	25.9	9.10	159	579	953	1743	9773	5	0.4	14	212	22.0	21.9	909
8.1	om	2198	0.47	71	4.6	9.9	4.43	70	233	368	626	9515	26	0.5	11	7	15.4	15.3	866
2.1	om	960	2.27	86	6.0	8.1	3.61	37	111	159	295	8021	13	0.6	10	216	14.8	14.6	861
4.1	c	901	0.08	14	4.4	7.9	1.36	46	115	142	199	8397	12	0.2	5	1	23.5	23.0	918
6.1	om	185	0.01	6	0.1	0.2	0.12	2	13	34	104	9828	134	0.5	63	5	1.7	1.7	655
12.1	c	799	0.23	25	4.5	7.8	1.48	39	97	124	195	8424	13	0.3	6	17	10.4	10.2	822
Sample 13-43																			
7.1	c	323	9.34	21	0.8	0.9	0.49	5	21	50	138	6219	4	0.7	33	15	3.2	3.0	706
1.1		226	0.06	33	1.5	2.5	1.20	13	29	37	60	7765	61	0.6	6	0	14.7	14.7	861
4.1	c/om	217	0.03	3	0.1	0.2	0.25	3	15	42	104	10 694	32	1.0	40	7	3.9	4.2	724
2.1	om	263	0.03	1	0.1	0.5	0.10	5	27	41	73	11 275	12	0.2	17	7	5.0	5.0	748
5.1	om/r	1360	0.04	52	1.5	4.3	1.65	31	129	238	466	9846	117	0.4	18	10	10.1	10.0	819
6.1	om	806	0.04	14	0.2	1.1	0.36	14	68	140	304	11 931	79	0.3	26	51	3.4	3.6	713
3.1	om	1154	0.28	107	7.6	12.0	4.19	58	136	180	283	9235	39	0.5	6	4	26.4	25.7	933
Sample 13-27																			
2.1	om	5740	1.90	54	36.4	96.7	58.89	581	1,039	666	796	7825	3	0.8	2	1252	108.8	108.7	1153
4.1	om	4509	1.32	41	19.6	61.7	39.52	427	721	554	716	10 709	4	0.7	2	1375	73.8	72.7	1085
5.1	om	1798	0.16	34	4.9	8.1	3.42	53	189	304	499	9591	21	0.5	12	2	35.6	35.2	974
3.1	c	1414	0.02	9	1.7	4.4	0.86	43	149	244	410	9469	26	0.2	12	24	11.7	12.7	835
1.1	om	832	0.02	19	0.5	1.8	0.12	18	81	147	266	9175	94	0.06	18	5	8.7	8.7	802
7.1		1969	1.83	75	5.4	10.2	3.16	69	211	325	539	8888	13	0.4	10	2	25.1	25.0	926
6.1	c	1171	0.03	92	1.6	3.4	1.53	28	114	210	415	9170	245	0.5	18	3	10.1	9.9	818
Sample VL10-01																			
4.1	c	0.054	13	4.3	8.7	0.83	57	149	1397	230	381	11 448	28	0.11	8				
2.1	c	0.175	65	1.3	2.5	1.12	21	74	871	154	332	10 874	92	0.47	20				
3.1	c	0.017	29	0.5	1.1	0.57	10	43	703	123	360	11 369	263	0.53	43				
5.1	c	0.019	23	2.3	4.9	1.38	30	78	724	115	206	10 668	116	0.35	8				
1.1	c	0.018	17	0.4	0.9	0.56	8	36	482	87	231	10 109	167	0.62	35				

Note: All analyses were performed on the SHRIMP-RG ion microprobe at the United States Geological Survey-Stanford University Microanalytical Center, Stanford, California following procedure outlined in Mazdab and Wooden (2006). All abundances expressed in parts per million (ppm).
[a]CL (cathodoluminescence) designations: om = oscillatory zoned mantle, c = core, r = rim.

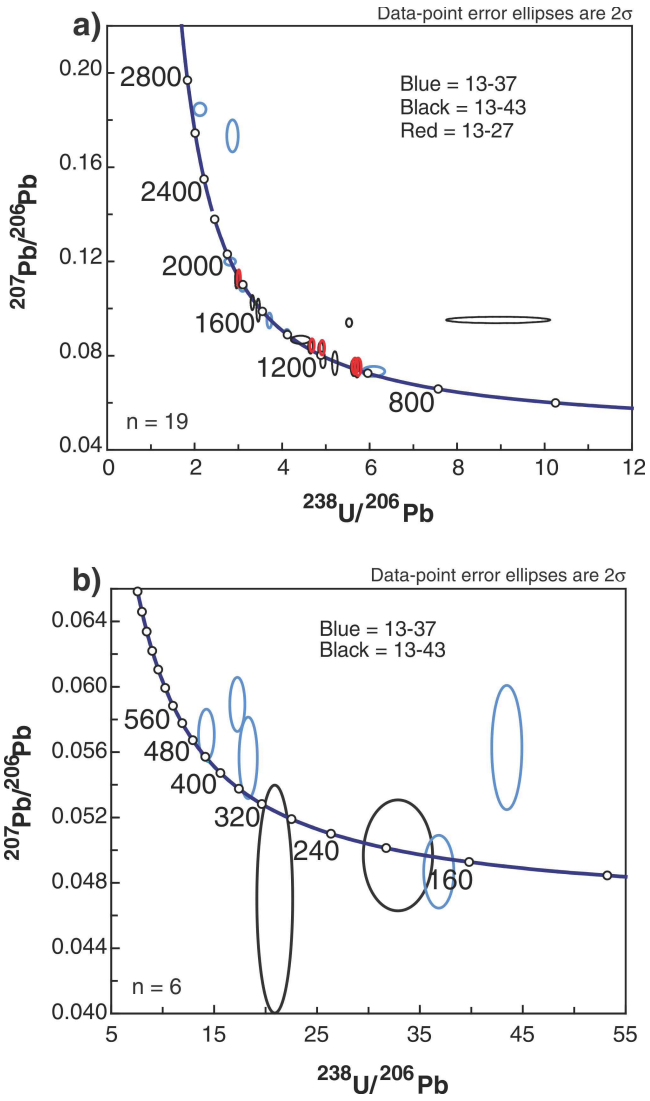

Figure 9. Tera-Wasserburg plots of SHRIMP-RG U-Pb data of zircon combining all the analyses from the three Tower Peak metabasalt samples: **a)** grains older than 600 Ma; **b)** grains younger than 600 Ma. The plotted data are uncorrected for ^{204}Pb.

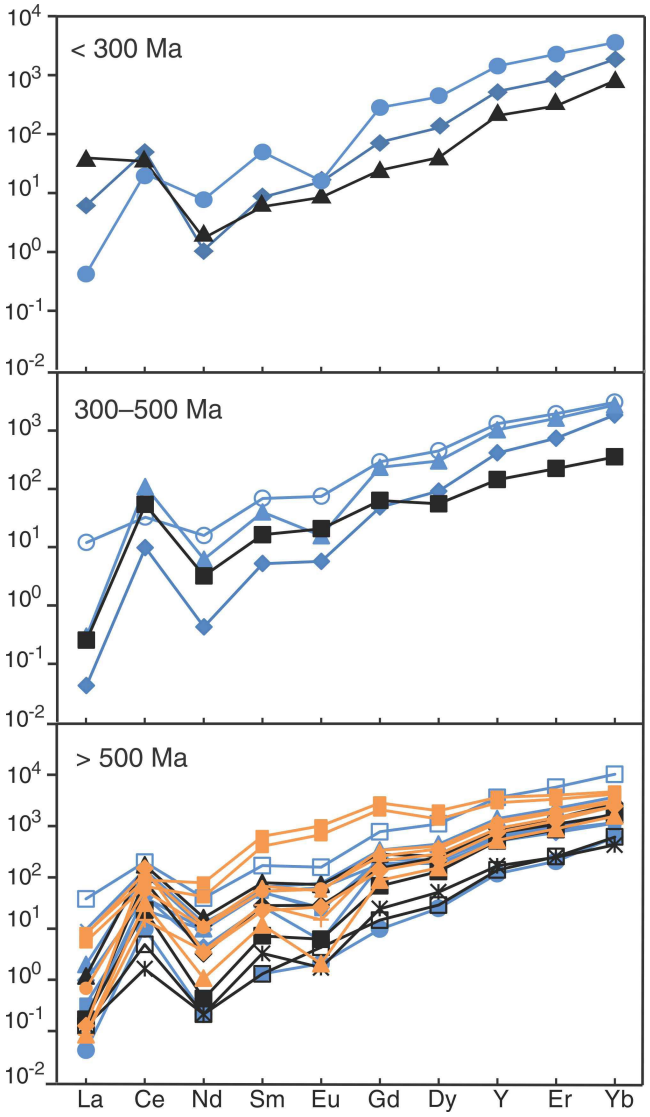

Figure 10. Chondrite-normalized REE patterns for the different age populations of zircon in the Tower Peak unit, colour coded by sample (13-37 blue, 13-43 black, 13-27 orange).

The youngest group consists of three grains with ^{207}Pb-corrected ^{206}Pb-^{238}U ages of 146 Ma, 173 Ma, and 198 Ma (Fig. 9b). The 173 Ma and 198 Ma ages are concordant, whereas the 146 Ma grain is discordant due to higher common Pb. Two grains (11 from sample 13-17 and 7 from sample 13-43) are cathodoluminescence-bright and euhedral with well developed oscillatory zoning. Grain 9 (sample 13-37) is a cathodoluminescence-dark zircon fragment with a truncated cathodoluminescence-light zone. These zircon grains have a positive Ce anomaly, a slightly negative Eu anomaly, steep HREE pattern (Yb/Gd = 10–27; Fig. 10), and Th/U ratios of 0.4. Ti-in-zircon temperatures range from 706°C to 850°C (Fig. 11).

Gabbro VL10-01

Five small (50–75 µm), euhdral to subhedral zircon grains were recovered from VL10-01. The ^{207}Pb-corrected $^{206}Pb/^{238}U$ ages of the five grains are 123 Ma, 126 Ma, 158 Ma, 177 Ma, and 189 Ma (Fig. 12). Grain 2 has a cathodoluminescence-light core with a subhedral shape and several inclusions, and a cathodoluminescence-dark rim. Grain 4 has a diffuse cathodoluminescence-grey core with a cathodoluminescence-light homogenous rim. Grain 3.1 is subhedral with alternating cathodoluminescence-dark and medium grey zoning. Grain 5 is cathodoluminescence-light with poorly developed zoning. The grain has a subrounded morphology. Grain 1 is euhedral with well developed, cathodoluminescence-moderate to -dark oscillatory zoning. Trace elements exhibit a positive Ce-anomaly, a slight negative Eu-anomaly, and steep HREEs (Yb/Gd = 8–43; Fig. 12).

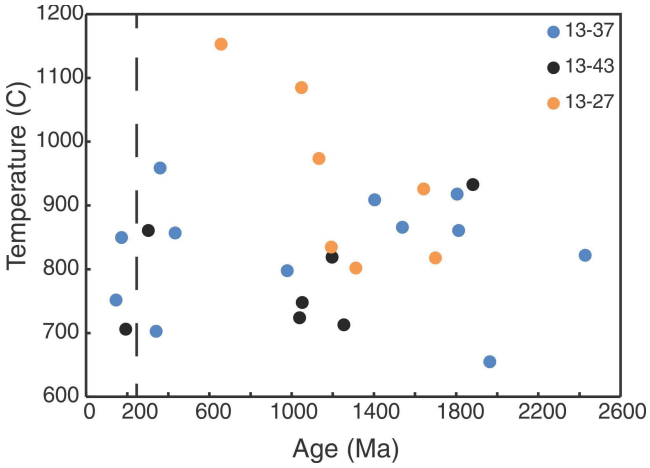

Figure 11. Ti-in-zircon temperature versus age for three Tower Peak metabasalt samples.

URANIUM-LEAD DETRITAL ZIRCON GEOCHRONOLOGY OF MARBLE UNIT

Analytical method

Zircon was extracted from marble sample 13-25 from the prominent ridge exposed in the footwall of the St. Cyr klippe using identical mineral separation procedures described above. Grains were imaged by cathodoluminescence on the Hitachi S3400 SEM at the University of Iowa to define intragrain complexities and aid in spot selection. The zircon grains were analyzed for U-Th-Pb by laser ablation multi-collector inductively coupled plasma mass spectrometry (LA-MC-ICPMS) using the Nu Instruments HR ICPMS and Photon Machines Analyte G2 excimer laser at the University of Arizona LaserChron Center, Tucson, Arizona. Standards were analyzed at the beginning, end, and after every five grains for the primary standard (SL) and after every 15 grains for the secondary standard (R33). Spot size was 30 µm. Analytical procedures follow Gehrels et al. (2006, 2008). The data are presented in Table 4.

Results

Detrital zircon U-Pb geochronology was employed to place a maximum depositional age on a coarse-grained marble located at the northern end of the study area (Fig. 3), and aid in identifying the primary sources of sediment during deposition. Marble sample 13-25 yielded 32 detrital zircon grains that are colourless and 50–100 µm long. Many of the grains show euhedral boundaries, distinct cores, and oscillatory zoning. Zircon ages range from 1985 ± 14 Ma to 368 ± 6 Ma; the majority of zircon grains are older than 1000 Ma (Fig. 13). Three grains are greater than 10% discordant and are not plotted. Four distinct age populations are defined: 441–368 Ma, 635 Ma, 1486–1000 Ma, and

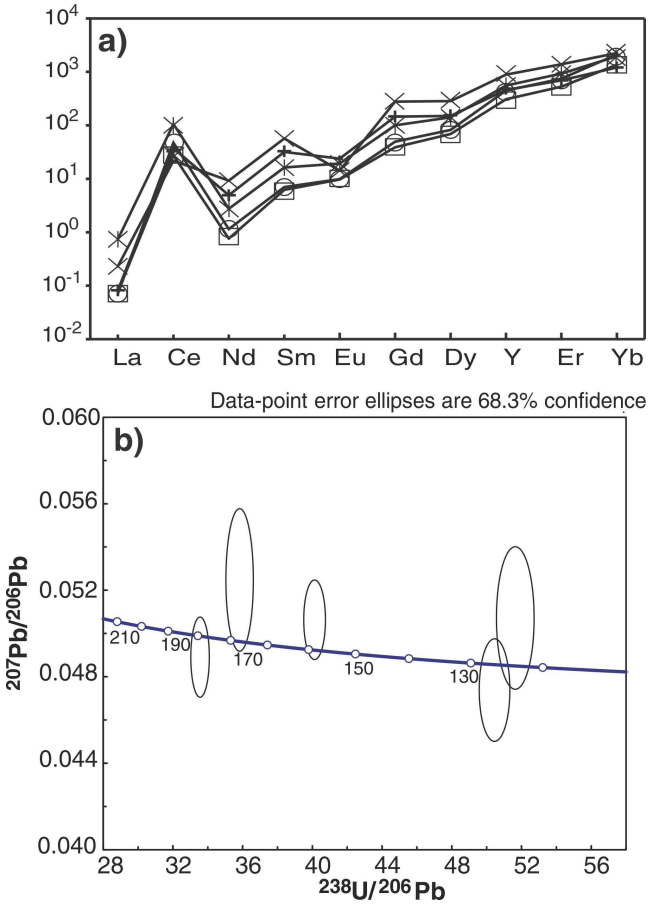

Figure 12. a) Chondrite-normalized REE patterns from zircon in gabbro sample VL10-01 and **b)** Tera-Wasserburg diagram of SHRIMP-RG U-Pb dates.

1985–1783 Ma. The maximum depositional age for the unit is provided by two methods (Dickinson and Gehrels, 2009): 1) the youngest single grain age of 368 ± 6 Ma or late Devonian, or 2) the three youngest overlapping concordant grains that give a weighted-mean age of 421 ± 8 Ma (2σ, MSWD = 1.5) or latest Silurian (Pridoli) using time scale of Walker et al. (2012).

DISCUSSION AND INTERPRETATION

Tower Peak unit

Mineralogical, petrological, and geochemical observations point to a basaltic protolith for the fine-grained, massive rocks of the Tower Peak unit. The absence of primary features compounds the difficulty of identifying the origin of these rocks; however, the relatively large crystals of interlocking plagioclase and pyroxene (Fig. 4c) suggest a former diabase that could have been a dyke, sill, or phenocrysts in a hypabyssal intrusion. Trace-element geochemistry from two samples is that of N-MORB, whereas two other samples plot

Table 4. Detrital zircon data for sample 13-25 (UTM zone 8V: E 0600722 m, N 6806387 m).

Analysis	U (ppm)	Th/U	$^{206}Pb^*$ $^{207}Pb^*$	± (%)	$^{207}Pb^*/^{235}U^*$	± (%)	$^{206}Pb^*/^{238}U$	± (%)	error corr.	$^{206}Pb^*/^{238}U^*$	± (Ma)	$^{207}Pb^*/^{235}U$	± (Ma)	$^{206}Pb^*/^{207}Pb^*$	± (Ma)	Best age (Ma)	± (Ma)	Conc (%)
1	922	0.11	18.5436	1.8	0.4370	2.5	0.0588	1.7	0.68	368	6	368	8	368	42	368	6	NA
9	195	0.27	17.9978	5.0	0.4885	6.2	0.0638	3.7	0.60	398	14	404	21	435	111	398	14	NA
19	314	0.77	18.5059	4.9	0.5025	5.2	0.0674	1.9	0.36	421	8	413	18	373	110	421	8	NA
4	294	0.41	18.6398	3.2	0.5037	3.4	0.0681	1.3	0.37	425	5	414	12	356	71	425	5	NA
32	229	0.58	17.9275	3.6	0.5447	3.8	0.0708	1.3	0.33	441	5	442	14	444	80	441	5	NA
16	111	0.63	16.5107	5.6	0.8641	5.9	0.1035	1.9	0.32	635	11	632	28	624	121	635	11	NA
23	145	0.35	13.7899	1.7	1.7087	2.7	0.1709	2.0	0.76	1017	19	1012	17	1000	35	1000	35	102
26	228	0.61	13.3170	1.3	1.8819	1.7	0.1818	1.0	0.61	1077	10	1075	11	1071	26	1071	26	101
3	148	0.67	13.2486	1.9	1.9322	2.3	0.1857	1.3	0.58	1098	13	1092	15	1081	37	1081	37	102
18	214	0.26	13.2242	1.4	1.9132	1.9	0.1835	1.2	0.65	1086	12	1086	13	1085	29	1085	29	100
29	423	0.42	13.2172	0.9	1.9075	1.9	0.1829	1.7	0.89	1083	17	1084	13	1086	18	1086	18	100
22	218	0.59	13.1419	1.3	1.9080	1.8	0.1819	1.2	0.69	1077	12	1084	12	1098	26	1098	26	98
15	239	0.14	13.1148	1.2	1.9698	1.9	0.1874	1.4	0.78	1107	15	1105	13	1102	23	1102	23	100
17	449	0.11	12.8068	0.8	2.0060	1.4	0.1863	1.2	0.84	1101	12	1118	10	1149	15	1149	15	96
31	114	0.58	12.7614	2.2	2.0410	2.9	0.1889	1.9	0.66	1115	20	1129	20	1156	43	1156	43	96
28	131	0.44	12.6374	1.9	2.2315	2.6	0.2045	1.8	0.68	1200	20	1191	18	1175	38	1175	38	102
11	105	0.82	12.5660	2.2	2.2188	2.6	0.2022	1.3	0.51	1187	14	1187	18	1187	44	1187	44	100
24	270	0.23	11.9913	0.7	2.5502	2.2	0.2218	2.1	0.95	1291	24	1286	16	1278	13	1278	13	101
13	448	0.38	11.9299	0.6	2.3575	4.5	0.2040	4.4	0.99	1197	48	1230	32	1288	12	1288	12	93
33	260	0.30	11.8338	1.0	2.4073	1.4	0.2066	1.0	0.71	1211	11	1245	10	1304	20	1304	20	93
7	234	0.76	11.5658	0.7	2.5288	3.7	0.2121	3.6	0.98	1240	41	1280	27	1349	14	1349	14	92
14	166	0.28	11.3162	1.6	2.7096	5.4	0.2224	5.2	0.96	1294	61	1331	40	1390	30	1390	30	93
5	238	0.27	10.9637	0.5	3.2204	1.3	0.2561	1.2	0.92	1470	16	1462	10	1451	10	1451	10	101
30	330	0.56	10.7698	0.5	3.4118	1.3	0.2665	1.2	0.92	1523	16	1507	10	1485	10	1485	10	103
27	262	0.70	10.7617	0.6	3.3219	1.4	0.2593	1.2	0.89	1486	16	1486	11	1486	12	1486	12	100
10	507	0.20	9.1723	0.4	4.8609	2.9	0.3234	2.9	0.99	1806	46	1796	25	1783	7	1783	7	101
25	257	0.49	8.8157	0.5	4.7754	1.5	0.3053	1.4	0.94	1718	22	1781	13	1855	9	1855	9	93
21	196	0.77	8.5006	0.5	5.6636	1.4	0.3492	1.4	0.95	1931	23	1926	12	1921	8	1921	8	101
8	143	0.58	8.2020	0.8	6.1122	1.6	0.3636	1.4	0.88	1999	24	1992	14	1985	14	1985	14	101
Rejected due to greater than 10% discordance, greater than 5% reverse discordance, or greater than 10% 2σ uncertainty in age																		
6	692	0.18	17.9040	2.0	0.5397	5.7	0.0701	5.4	0.94	437	23	438	20	447	45	437	23	NA
20	298	0.33	23.9670	31.3	0.0505	32.3	0.0088	8.2	0.25	56	5	50	16	-243	807	56	5	NA
34	57	0.84	13.2572	4.3	1.7987	4.8	0.1729	2.1	0.44	1028	20	1045	31	1080	87	1080	87	95

1. All uncertainties are reported at the 1σ level, and include only measurement errors. Systematic errors would increase the uncertainty of clusters of ages by 1–2%.
2. U concentration and U/Th are calibrated relative to Arizona Laserchron in-house Sri Lanka zircon and are accurate to about 20%.
3. Common Pb correction is from ^{204}Pb, with composition interpreted from Stacey and Kramers (1975) and uncertainties of 1.0 for $^{206}Pb/^{204}Pb$, 0.3 for $^{207}Pb/^{204}Pb$, and 2.0 for $^{208}Pb/^{204}Pb$; error corr. = error correction.
4. U/Pb and $^{206}Pb/^{207}Pb$ fractionation is calibrated relative to fragments of a large Sri Lanka zircon of 563.5 ± 3.2 Ma (2σ).
5. U decay constants and composition as follows: $^{238}U = 9.8485 \times 10^{-10}$, $^{235}U = 1.55125 \times 10^{-10}$, $^{238}U/^{235}U = 137.8$
6. Best age is determined from $^{206}Pb/^{238}U$ age for analyses with $^{206}Pb/^{238}U$ age less than 1000 Ma and from $^{206}Pb/^{207}Pb$ age for analyses with $^{206}Pb/^{238}U$ age greater than 1000 Ma.
7. Concordance (Conc) is based on $^{206}Pb/^{238}U$ age / $^{206}Pb/^{207}Pb$ age. Value is not reported for $^{206}Pb/^{238}U$ ages less than 600 Ma because of large uncertainty in $^{206}Pb/^{207}Pb$ age.

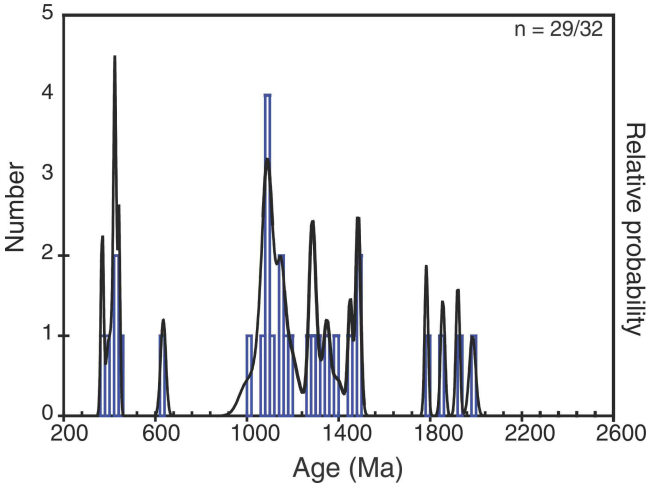

Figure 13. Plot of the number of grains and relative probability versus age for grains that are less than 10% discordant. The youngest grain is 368 Ma. The plotted data are corrected for ^{204}Pb. Grains younger than 1000 Ma use the $^{238}U/^{206}Pb$ age; older grains report the $^{207}Pb/^{206}Pb$ age.

in the arc-basalt field (Fig. 5c). Enrichment in Th and LILEs may reflect crustal contamination or fluid alteration during brecciation.

Tectonic settings that could combine an arc and MORB signature are back-arc basin and island-arc basalt. Back-arc basins typically have MORB signatures with a slight subduction influence (Pearce, 2008), which could account for the enriched signatures. Island-arc basalt units are typically enriched, but do not always have signatures that deviate from N-MORB (Woodhead et al., 1993). An island-arc interpretation fits well with the high concentrations of LILEs relative to HFSEs seen in all the samples (Pearce and Peate, 1995). The two different geochemical features could also be attributed to variable degrees of partial melting in a single island-arc or back-arc tectonic environment. The small sample size precludes a more robust interpretation based on geochemistry alone.

The zircon population extracted from three metabasalt samples from the Tower Peak unit displays a wide array of ages, and is more similar to an inherited xenocrystic population than magmatic zircon that defines a single crystallization event. All three samples yielded zircon with overlapping Precambrian ages, and two of the three Tower Peak samples contain a few Paleozoic and Mesozoic grains, demonstrating that the heterogeneous zircon population is characteristic of the Tower Peak basalt. The Precambrian grains are rounded—more typical of sedimentary recycling than inherited igneous xenocrysts—whereas Paleozoic and Mesozoic grains are mostly euhedral. Grains older than 1600 Ma are commonly attributed to Laurentian basement (Gehrels et al., 1995; Gehrels and Ross, 1998; Piercey and Colpron, 2009); such grains occur in the Devonian and older sedimentary rocks that form the substrate to the Yukon-Tanana terrane (Colpron et al., 2005). Grains with ages between 1000 Ma and 1300 Ma occur throughout the Cordillera and may represent recycled material from the Grenville Orogen that was deposited in the northern Cordillera in the Proterozoic and reworked throughout the Paleozoic (Rainbird et al., 1997; Gehrels and Pecha, 2014).

Many of the mafic and ultramafic units in the St. Cyr area have been attributed to the Paleozoic Slide Mountain terrane (Colpron, 2006). If the Tower Peak basalts were associated with the Slide Mountain Ocean, then one would expect to see zircon ages between late Devonian and Triassic (Nelson et al., 2013). Three grains give ages in this range (360 ± 6 Ma, 341 ± 7 Ma and 303 ± 4 Ma); the two older grains have oscillatory zoning, are euhedral and appear to be magmatic. Their positive Ce anomaly, negative Eu anomaly and Th/U ratios ranging from 0.1–1.4 are also consistent with an igneous origin; however, three grains with an age spread from Lower to Upper Jurassic (193 ± 8 Ma, 173 ± 3 Ma, 146 ± 2 Ma) are also euhedral, oscillatory zoned and retain trace-element signatures that fit an igneous origin. A population of five concordant Mesozoic grains was also unexpectedly retrieved from gabbro sample VL10-01 with grains as young as Lower Cretaceous. The results were so surprising that the authors checked the sample processing records from the Mineral Separation Lab (University of Iowa) for possible contamination. The samples were processed at different times and no other rocks had Mesozoic grains, so contamination during processing is considered highly improbable.

An interpretation of this zircon population is difficult because of the low number of grains and the lack of overlap among any of the ages. The simplest (and preferred) interpretation is that the zircon grains are inherited grains that were entrained in the mafic magmas during emplacement, and that the minimum intrusive age for the Tower Peak unit is after 146 Ma or Upper Jurassic. A post–Lower Cretaceous age is possible given that the youngest grain in the gabbro is 123 ± 1.8 Ma.

One could argue that the Paleozoic zircon grains fit with an anticipated Slide Mountain Ocean age, and that the young ages are metamorphic or hydrothermal. A metamorphic origin for the Mesozoic zircon grains is considered unlikely for several reasons. First, the Th/U ratios are too high (~0.4), and resemble values expected for igneous zircon (~0.5; Rubatto, 2002; Hoskin and Schaltegger, 2003). Second, the cathodoluminescence images do not reveal any obvious overgrowths or rims except for grains 10 (sample 13-37) and 6 (sample 13-43), which have very thin dark rims that are too small to analyze. Third, Ti-in-zircon temperatures range from 706–850°C, which contradicts the petrological evidence for greenschist-facies metamorphism. A hydrothermal origin for the zircon is also considered unlikely, despite the abundant crosscutting veins in the area. Hydrothermal zircon can be difficult to identify because REE patterns can be enriched or depleted (Hoskin et al., 1998; Schaltegger et al., 2001). The most definitive indicator of a hydrothermal origin is a spongy texture due to fluid inclusions in zircon (Hoskin et al., 1998; Hoskin and Schaltegger, 2003); however, zircon

from the Tower Peak unit does not contain any obvious fluid inclusions. Furthermore, the Ti-in-zircon temperatures (706–850°C) are more indicative of mafic igneous zircon (Fu et al., 2008) rather than hydrothermal zircon with temperatures below 500°C (Fu et al., 2009).

Nelson et al. (2013 and references therein) outline the history of accretion and obduction of the Peri-Laurentian realm, including Yukon-Tanana terrane, with North America and the subsequent amalgamation of outboard terranes with the Peri-Laurentian realm. A Jurassic age for the Tower Peak unit severs any potential ties to Yukon-Tanana terrane and its associated back-arc basins, as both arc and oceanic magmatism are interpreted to have ceased by the Permian, as evidenced by Permo-Triassic sedimentary rocks in western Yukon (Beranek et al., 2010a, Beranek and Mortensen, 2011). Stikinia and Quesnellia are both Peri-Laurentian terranes with components of Jurassic arc rocks; these are possible candidates for providing the zircon populations seen in the Tower Peak unit. In Stikinia, the Hazelton Group is composed of lower to middle Jurassic volcanic and sedimentary strata that represent the last gasp of volcanism (MacIntyre et al., 2001). The Rossland Group of Quesnellia also consists of lower to middle Jurassic volcanic and sedimentary units (Beatty et al., 2006). Alternatively, fleeting back-arc basins associated with Quesnellia or Stikinia could also be the source of the Tower Peak unit.

Correlation of the footwall marble with the Yukon-Tanana terrane Finlayson assemblage

The detrital zircon ages in the marble indicate derivation from a variety of sources. Similar to the Tower Peak unit, grains older than 1700 Ma are attributed to Laurentian basement provinces, whereas grains with ages ranging from 1000–1300 Ma are thought to represent recycled detritus from the Grenville Orogen. The provenance of the 420–441 Ma ages are debatable, but grains of this age have been documented in northern British Columbia and attributed to the Franklinian or Caledonian clastic wedges (Gehrels and Pecha, 2014). The 398 Ma and 368 Ma grains are most likely coeval with the magmatic development of the Yukon-Tanana terrane (Nelson and Gehrels, 2007). The maximum depositional age from the youngest single grain is 368 Ma. Additional data are needed to more rigorously discuss the maximum depositional age for this unit (e.g. Dickinson and Gehrels, 2009). Nevertheless, the correlation of the marble to the lower Cambrian Scurvy limestone from the Cassiar terrane (i.e. the Laurentian miogeocline) proposed by Tempelman-Kluit (2012) is precluded by the detrital zircon data. Marble and calcareous phyllite of Devonian age have been correlated with the Finlayson assemblage in the Drury Formation, Glenlyon area (Colpron et al., 2002; Colpron, 2006). The present authors interpret the marble unit in the footwall of the St. Cyr klippe to be part of the Finlayson assemblage, the oldest arc assemblage in the Yukon-Tanana terrane. Alternatively, the detrital zircon signature is broadly similar to that observed in Devonian-Mississipian strata on the northern Cordilleran margin (Beranek et al., 2010a, b), suggesting a possible correlation with strata originating east of the Slide Mountain ocean.

FUTURE WORK

This study illustrates the danger in the common assumption that all mafic-ultramafic complexes associated with Yukon-Tanana terrane are somehow part of the Slide Mountain terrane. The Mesozoic history of terrane accretion may also be recorded by bits of oceanic crust, and back-arc and island-arc material that were added to Yukon-Tanana terrane as it was thrust onto North America, probably from the Pacific Realm. These results from the Tower Peak unit may be better understood if future work turns up more Jurassic zircon in other mafic units. Much more geochronology is needed to better understand the tectonic evolution of the mafic-ultramafic rocks that have been mapped as Slide Mountain terrane.

ACKNOWLEDGMENTS

This study is based on a M.Sc. thesis by S.J. Isard. The authors thank N. Lamkey for his help as a field assistant, and the Yukon Geological Survey for their logistical support. M. Coble provided student training, advice, and insightful discussion during the analytical sessions at the Stanford–U.S. Geological Survey Micro Analysis Center. The project was funded by National Science Foundation grant EAR1118834 to J.A. Gilotti; a Canadian Northern Economic Development Agency grant through the Yukon Geological Survey, a Geological Society of America Student Research Grant, the Littlefield Fund of the Department of Earth and Environmental Sciences and the Central Microscopy Research Facility, University of Iowa to S.J. Isard; and Geological Survey of Canada funding to C.R. van Staal and W.C. McClelland. Detrital zircon analysis was partially funded by National Science Foundation grant EAR 1338583 to the University of Arizona Laserchron Center. The authors thank J. Ryan for his careful review of the manuscript.

REFERENCES

Barth, A.P. and Wooden, J.L., 2006. Timing of magmatism following initial convergence at a passive margin, southwestern US Cordillera, and ages of lower crustal magma sources; The Journal of Geology, v. 114, no. 2, p. 231–245. doi:10.1086/499573

Barth, A.P. and Wooden, J.L., 2010. Coupled elemental and isotopic analyses of polygenetic zircons from granitic rocks by ion microprobe, with implications for melt evolution and the sources of granitic magmas; Chemical Geology, v. 277, p. 149–159. doi:10.1016/j.chemgeo.2010.07.017

Beatty, T.W., Orchard, M.J., and Mustard, P.S., 2006. Geology and tectonic history of the Quesnel terrane in the area of Kamloops, British Columbia; *in* Paleozoic Evolution and Metallogeny of Pericratonic Terranes at the Ancient Pacific Margin of North America, Canadian and Alaskan Cordillera, (ed.) M. Colpron and J.L. Nelson; Geological Association of Canada, Special Paper 45, p. 483–504.

Beranek, L. and Mortensen, J., 2011. The timing and provenance record of the Late Permian Klondike orogeny in northwestern Canada and arc-continent collision along western North America; Tectonics, v. 30, cit. no. TC5017. doi:10.1029/2010TC002849

Beranek, L., Mortensen, J., Orchard, M., and Ullrich, T., 2010a. Provenance of North American Triassic strata from west-central and southeastern Yukon: correlations with coeval strata in the Western Canada Sedimentary Basin and Canadian Arctic Islands; Canadian Journal of Earth Sciences, v. 49, no. 1, p. 53–73.

Beranek, L.P., Mortensen, J.K., Lane, L.S., Allen, T.L., Fraser, T.A., Hadlari, T., and Zantvoort, W.G., 2010b. Detrital zircon geochronology of the western Ellesmerian clastic wedge, northwestern Canada; insights on Arctic tectonics and the evolution of the northern Cordilleran miogeocline; Geological Society of America Bulletin, v. 122, p. 1899–1911. doi:10.1130/B30120.1

Black, L.P., Kamo, S.L., Allen, C.M., Davis, D.W., Aleinikoff, J.N., Valley, J.W., Mundil, R., Campbell, I.H., Korsh, R.J., Williams, I.S., and Foudoulis, C., 2004. Improved $^{206}Pb/^{238}U$ microprobe geochronology by monitoring of a trace-element-related matrix effect; SHRIMP, ID-TIMS, ELA-ICP-MS and oxygen isotope documentation for a series of zircon standards; Chemical Geology, v. 205, p. 115–140. doi:10.1016/j.chemgeo.2004.01.003

Colpron, M., 2006. Tectonic assemblage map of Yukon-Tanana and related terranes in Yukon and northern British Columbia; Yukon Geological Survey, Open File 2006-1, scale 1:1 000 000.

Colpron, M., Murphy, D.C., Nelson, J.L., Roots, C.F., Gladwin, K., Gordey, S.P., and Abbott, J.G., 2002. Yukon targeted geoscience initiative, Part 1: results of accelerated bedrock mapping in Glenlyon (105L/1–7, 11–14) and northeast Carmacks (115I/9, 16) areas, central Yukon; Yukon Exploration and Geology, p. 85–108.

Colpron, M., Gladwin, K., Johnston, S.T., Mortensen, J.K., and Gehrels, G.E., 2005. Geology and juxtaposition history of Yukon-Tanana, Slide Mountain and Cassiar terranes in the Glenlyon area of central Yukon; Canadian Journal of Earth Sciences, v. 42, p. 1431–1448. doi:10.1139/e05-046

Colpron, M., Nelson, J.L., and Murphy, D.C., 2006. A tectonostratigraphic framework for the pericratonic terranes of the northern Canadian Cordillera; *in* Paleozoic Evolution and Metallogeny of Pericratonic Terranes at the Ancient Pacific Margin of North America, Canadian and Alaskan Cordillera, (ed.) M. Colpron and J.L. Nelson; Geological Association of Canada, Special Publication 45, p. 1–23.

Colpron, M., Nelson, J.L., and Murphy, D.C., 2007. Northern Cordillera terranes and their interactions through time; GSA Today, v. 17, no. 4/5. doi:10.1130/GSAT01704-5A.1

Colpron, M., Crowley, J.L., Gehrels, G., Long, D.G.F., Murphy, D.C., Beranek, L., and Bickerton, L., 2015. Birth of the northern Cordilleran orogeny, as recorded by detrital zircons in Jurassic synorogenic strata and regional exhumation in Yukon; Lithosphere, v. 7, p. 541–562. doi:10.1130/L451.1

Devine, F., Murphy, D.C., Kennedy, R., Tizzard, A.M., and Carr, S.D., 2004. Geological setting of retrogressed eclogite and jade in the southern Campbell Range: preliminary structure and stratigraphy, Frances Lake area (NTS 105H), southeastern Yukon; *in* Yukon Exploration and Geology 2003, (ed.) D.S. Emond and L.L. Lewis; Yukon Geological Survey, p. 89–105.

Dickinson, W.R. and Gehrels, G.E., 2009. Use of U-Pb ages of detrital zircons to infer maximum depositional ages of strata: a test against a Colorado Plateau Mesozoic database; Earth and Planetary Science Letters, v. 288, p. 115–125. doi:10.1016/j.epsl.2009.09.013

Erdmer, P., 1992. Eclogitic rocks of the St. Cyr klippe, Yukon, and their tectonic significance; Canadian Journal of Earth Sciences, v. 29, p. 1296–1304. doi:10.1139/e92-103

Evans, B.W., Hattori, K., and Baronnet, A., 2013. Serpentinite: what, why, where; Elements, v. 9, no. 2, p. 99–106. doi:10.2113/gselements.9.2.99

Fallas, K., Erdmer, P., Creaser, R., Archibald, D., and Heaman, L., 1999. New terrane interpretation for the St. Cyr Klippe, south-central Yukon; LITHOPROBE Slave-Northern Cordillera Lithospheric Evolution (SNORCLE) Transect Meeting Report, March 5–7, 1999, University of Calgary, Alberta, v. 69, p. 130–137.

Ferry, J.M. and Watson, E.B., 2007. New thermodynamic models and revised calibrations for the Ti-in-zircon and Zr-in-rutile thermometers; Contributions to Mineralogy and Petrology, v. 154, p. 429–437. doi:10.1007/s00410-007-0201-0

Fu, B., Page, F.Z., Cavosie, A.J., Fournelle, J., Kita, N.T., Lackey, J.S., and Valley, J.W., 2008. Ti-in-zircon thermometry: applications and limitations; Contributions to Mineralogy and Petrology, v. 156, p. 197–215. doi:10.1007/s00410-008-0281-5

Fu, B., Mernagh, T.P., Kita, N.T., Kemp, A.I., and Valley, J.W., 2009. Distinguishing magmatic zircon from hydrothermal zircon: a case study from the Gidginbung high-sulphidation Au-Ag-(Cu) deposit, SE Australia; Chemical Geology, v. 259, p. 131–142. doi:10.1016/j.chemgeo.2008.10.035

Gabrielse, H., Murphy, D.C., and Mortensen, J.K., 2006. Cretaceous and Cenozoic dextral orogen-parallel displacements, magmatism, and paleogeography, north-central Canadian Cordillera; paleogeography of the North American Cordillera: evidence for and against large-scale displacements; *in* Evidence for Major Lateral Displacements in the North American Cordillera, (ed.) J.W. Haggart, J.W.H. Monger, and R.J. Enkin; Geological Association of Canada, Special Paper 46, p. 255–276.

Gehrels, G. and Pecha, M., 2014. Detrital zircon U-Pb geochronology and Hf isotope geochemistry of Paleozoic and Triassic passive margin strata of western North America; Geosphere, v. 10, p. 49–65. doi:10.1130/GES00889.1

Gehrels, G.E. and Ross, G.M., 1998. Detrital zircon geochronology of Neoproterozoic to Permian miogeoclinal strata in British Columbia and Alberta; Canadian Journal of Earth Sciences, v. 35, p. 1380–1401. doi:10.1139/e98-071

Gehrels, G.E., Dickinson, W.R., Ross, G.M., Stewart, J.H., and Howell, D.G., 1995. Detrital zircon reference for Cambrian to Triassic miogeoclinal strata of western North America; Geology, v. 23, p. 831–834. doi:10.1130/0091-7613(1995)023%3c0831:DZRFCT%3e2.3.CO%3b2

Gehrels, G.E., Valencia, V., and Pullen, A., 2006. Detrital zircon geochronology by laser ablation multicollector ICPMS at the Arizona Laserchron Center; Geochronology: Emerging Opportunities, Paleontological Society Short Course; Paleontological Society Papers, v. 12, p. 67–76.

Gehrels, G.E., Valencia, V.A., and Ruiz, J., 2008. Enhanced precision, accuracy, efficiency and spatial resolution of U-Pb ages by laser ablation-multicollector-inductively coupled plasma-mass spectrometry; Geochemistry Geophysics Geosystems, v. 9, p. 1–13. doi:10.1029/2007GC001805

Gilotti, J.A., McClelland, W.C., Petrie, M., and Van Staal, C.R., 2013. Interpreting subduction polarity from eclogite-bearing slices in accretionary orogens – a cautionary note from the Yukon–Tanana terrane; Geological Society of America; Program with Abstracts, Geological Society of America, Annual Meeting, Denver, Colorado, v. 45, no. 7, p. 442.

Hoskin, P.W.O. and Schaltegger, U., 2003. The composition of zircon and igneous and metamorphic petrogenesis; Reviews in Mineralogy and Geochemistry, v. 53, p. 27–62. doi:10.2113/0530027

Hoskin, P.W.O., Kinny, P.D., and Wyborn, D., 1998. Chemistry of hydrothermal zircon: investigating timing and nature of water-rock interaction; Water-Rock Interaction, v. 9, p. 545–548.

Isard, S.J., 2014. Origin of the Tower Peak unit in the St. Cyr area, Yukon, Canadian Cordillera; M.Sc. thesis, University of Iowa, Iowa City, Iowa, 68 p.

Isard, S.J. and Gilotti, J.A., 2014. Geology and jade prospects of the northern St. Cyr klippe (NTS 105F/6), Yukon; *in* Yukon Exploration and Geology 2013, (ed.) K.E. MacFarlane, M.G. Nordling, and P.J. Sack; Yukon Geological Survey, p. 69–77.

Ludwig, K.R., 2009. SQUID 2: a user's manual, Volume 2; Berkeley Geochronology Center, Special Publication; Berkley, California, 104 p.

MacIntyre, D.G., Villeneauve, M.E., and Schiarizza, P., 2001. Timing and tectonic setting of Stikine Terrane magmatism, Babine-Takla lakes area, central British Columbia; Canadian Journal of Earth Sciences, v. 38, p. 579–601. doi:10.1139/e00-105

MacLean, W.H., 1990. Mass chance calculations in altered rock series; Mineralium Deposita, v. 25, p. 44–49. doi:10.1007/BF03326382

Mattinson, J.M., 2010. Analysis of the relative decay constants of ^{235}U and ^{238}U by multi-step CA-TIMS measurements of closed-system natural zircon samples; Chemical Geology, v. 275, p. 186–198. doi:10.1016/j.chemgeo.2010.05.007

Mazdab, F.M. and Wooden, J.L., 2006. Trace element analysis in zircon by ion microprobe (SHRIMP-RG), technique and applications; Geochimica et Cosmochimica Acta, v. 70, p. A405. doi:10.1016/j.gca.2006.06.817

McClelland, W.C. and Gehrels, G.E., 1990. Geology of the Duncan Canal shear zone: evidence for Early to Middle Jurassic deformation of the Alexander terrane, southeastern Alaska; Geological Society of America Bulletin, v. 102, p. 1378–1392. doi:10.1130/0016-7606(1990)102%3c1378:GOTDCS%3e2.3.CO%3b2

Monger, J.W.H. and Price, R.A., 2002. The Canadian Cordillera: geology and tectonic evolution; Canadian Society of Exploration Geophysicists Recorder, v. 27, p. 17–36.

Monger, J.W.H., Price, R.A., and Tempelman-Kluit, D.J., 1982. Tectonic accretion and the origin of the two major metamorphic and plutonic welts in the Canadian Cordillera; Geology, v. 10, p. 70–75. doi:10.1130/0091-7613(1982)10%3c70:TAATOO%3e2.0.CO%3b2

Mortensen, J.K., 1992a. New U-Pb ages for the Slide Mountain Terrane in southeastern Yukon Territory; *in* Radiogenic Age and Isotopic Studies: Report 5; Geological Survey of Canada, Paper 91-2, p. 167–173. doi:10.4095/132922

Mortensen, J.K., 1992b. Pre-mid-Mesozoic tectonic evolution of the Yukon–Tanana terrane, Yukon and Alaska; Tectonics, v. 11, p. 836–853. doi:10.1029/91TC01169

Murphy, D.C., Mortensen, J.K., Piercey, S.J., Orchard, M.J., and Gehrels, G.E., 2006. Mid-Paleozoic to early Mesozoic tectonostratigraphic evolution of Yukon-Tanana and Slide Mountain terranes and affiliated overlap assemblages, Finlayson Lake massive sulphide district, southeastern Yukon; *in* Paleozoic Evolution and Metallogeny of Pericratonic Terranes at the Ancient Pacific Margin of North America, Canadian and Alaskan Cordillera, (ed.) M. Colpron and J.L. Nelson; Geological Association of Canada, Special Paper 45, p. 75–105.

Nelson, J.L., 1993. The Sylvester allochthon: Upper Paleozoic marginal-basin and island-arc terranes in northern British Columbia; Canadian Journal of Earth Sciences, v. 30, p. 631–643. doi:10.1139/e93-048

Nelson, J.L. and Bradford, J.A., 1993. Geology of the Midway-Cassiar area, northern British Columbia (104O, 104P); British Columbia Geological Survey, Bulletin 83, 94 p.

Nelson, J.L. and Gehrels, G., 2007. Detrital zircon geochronology and provenance of the southeastern Yukon-Tanana terrane; Canadian Journal of Earth Sciences, v. 44, p. 297–316. doi:10.1139/e06-105

Nelson, J.L., Colpron, M., Piercey, S.J., Dusel-Bacon, C., Murphy, D.C., and Roots, C.F., 2006. Paleozoic tectonic and metallogenic evolution of the pericratonic terranes in Yukon, northern British Columbia and eastern Alaska; *in* Paleozoic Evolution and Metallogeny of Pericratonic Terranes at the Ancient Pacific Margin of North America, Canadian and Alaskan Cordillera, (ed.) M. Colpron and J.L. Nelson; Geological Association of Canada, Special Paper 45, p. 323–360.

Nelson, J.L., Colpron, M., and Israel, S., 2013. The Cordillera of British Columbia, Yukon, and Alaska: tectonics and metallogeny. Tectonics, metallogeny, and discovery; *in* The North American Cordillera and Similar Accretionary Settings, (ed.) M. Colpron, T. Bissig, B.G. Rusk, and J.F.H. Thompson; Society of Economic Geologists, Special Publication, v. 17, p. 53–109.

Orchard, M.J., 2006. Late Paleozoic and Triassic conodont faunas of Yukon Territory and northern British Columbia and implications for the evolution of Yukon-Tanana terrane; *in* Paleozoic Evolution and Metallogeny of Pericratonic Terranes at the Ancient Pacific Margin of North America, Canadian and Alaskan Cordillera, (ed.) M. Colpron and J.L. Nelson; Geological Association of Canada, Special Paper 45, p. 229–260.

Pearce, J.A., 1996. A user's guide to basalt discrimination diagrams; *in* Trace Element Geochemistry of Volcanic Rocks: Applications for Massive Sulphide Exploration, (ed.) D.A. Wyman; Geological Association of Canada, Short Course Notes 12, p. 79–113.

Pearce, J.A., 2008. Geochemical fingerprinting of oceanic basalts with applications to ophiolite classification and the search for Archean oceanic crust; Lithos, v. 100, p. 14–48. doi:10.1016/j.lithos.2007.06.016

Pearce, J.A. and Cann, J.R., 1973. Tectonic setting of basic volcanic rocks determined using trace element analysis; Earth and Planetary Science Letters, v. 19, p. 290–300. doi:10.1016/0012-821X(73)90129-5

Pearce, J.A. and Peate, D.W., 1995. Tectonic implications of the composition of volcanic arc magmas; Annual Review of Earth and Planetary Sciences, v. 23, p. 251–285. doi:10.1146/annurev.ea.23.050195.001343

Petrie, M.B., Gilotti, J.A., McClelland, W.C., van Staal, C., and Isard, S.J., 2015. Geologic setting of eclogite-facies assemblages in the St. Cyr klippe, Yukon-Tanana terrane, Yukon, Canada; Geoscience Canada, v. 42, p. 327–350. doi:10.12789/geocanj.2015.42.073

Piercey, S.J. and Colpron, M., 2009. Composition and provenance of the Snowcap assemblage, basement to the Yukon-Tanana terrane, northern Cordillera: implications for Cordilleran crustal growth; Geosphere, v. 5, p. 439–464. doi:10.1130/GES00505.S3

Pigage, L.C., 2004. Bedrock geology compilation of the Anvil District (parts of NTS 105K/2, 3, 5, 6, 7 and 11), central Yukon; Yukon Geological Survey Bulletin, v. 15, 103 p.

Rainbird, R.H., McNicoll, V.J., Theriault, R.J., Heaman, L.M., Abbott, J.G., Long, D.G.F., and Thorkelson, D.J., 1997. Pan-continental river system draining Grenville Orogen recorded by U-Pb and Sm-Nd geochronology of Neoproterozoic quartzarenites and mudrocks, northwestern Canada; The Journal of Geology, v. 105, p. 1–17. doi:10.1086/606144

Rubatto, D., 2002. Zircon trace element geochemistry: partitioning with garnet and the link between U-Pb ages and metamorphism; Chemical Geology, v. 184, p. 123–138. doi:10.1016/S0009-2541(01)00355-2

Schaltegger, U., Audetat, A., Pettke, T., and Heinrich, C.A., 2001. Dating of magmatic and hydrothermal stages in a Sn-W-granite; Journal of Conference Abstracts, v. 6, p. 681.

Stacey, J.T. and Kramers, J.D., 1975. Approximation of terrestrial lead isotope evolution by a two-stage model; Earth and Planetary Science Letters, v. 26, p. 207–221. doi:10.1016/0012-821X(75)90088-6

Stipp, M., Stünitz, H., Heilbronner, R., and Schmid, S., 2002. The eastern Tonale fault zone: a 'natural laboratory' for crystal plastic deformation of quartz over a temperature range from 250 to 750°C; Journal of Structural Geology, v. 24, p. 1861–1884. doi:10.1016/S0191-8141(02)00035-4

Sun, S.S. and McDonough, W.F., 1989. Chemical and isotopic systematics of oceanic basalts: implications for mantle composition and processes; Geological Society Special Publication 42, p. 313–345.

Tempelman-Kluit, D.J., 1979. Transported cataclasite, ophiolite and granodiorite in Yukon: evidence of arc-continent collision; Geological Survey of Canada, Paper 79–14, 27 p. doi:10.4095/105928

Tempelman-Kluit, D.J., 2012. Geology of Quiet Lake and Finlayson Lake map areas, south-central Yukon – an early interpretation of bedrock stratigraphy and structure; Geological Survey of Canada, Open File 5487, 103 p., 13 sheets. doi:10.4095/291931

van der Heyden, P., 1992. A Middle Jurassic to Early Tertiary Andean-Sierran arc model for the Coast belt of British Columbia; Tectonics, v. 11, p. 82–97. doi:10.1029/91TC02183

Walker, J.D., Geisman, J.W., Bowring, S.D., and Babcock, L.E., (comp.), 2012. Geologic time scale, version 4.0, Geological Society of America.

Watson, E.B. and Harrison, T.M., 2005. Zircon thermometer reveals minimum melting conditions on earliest Earth; Science, v. 308, p. 841–844. doi:10.1126/science.1110873

Wheeler, J.O., Brookfield, A.J., Gabrielse, H., Monger, J.W.H., Tipper, H.W., and Woodsworth, G.J., 1991. Terrane map of the Canadian Cordillera; Geological Survey of Canada, Map 1713A, scale 1:2 000 000.

Williams, I.S., 1998. U-Th-Pb geochronology by ion microprobe; *in* Applications of Microanalytical Techniques to Understand Mineralizing Processes, (ed.) M.A. McKibben; Reviews in Economic Geology 7, p. 1–35.

Winchester, J.A. and Floyd, P.A., 1977. Geochemical discrimination of different magma series and their differentiation products using immobile elements; Chemical Geology, v. 20, p. 325–343. doi:10.1016/0009-2541(77)90057-2

Wood, D.A., 1980. The application of a Th–Hf–Ta diagram to problems of tectonomagmatic classification and to establishing the nature of crustal contamination of basaltic lavas of the British Tertiary Volcanic Province; Earth and Planetary Science Letters, v. 50, p. 11–30. doi:10.1016/0012-821X(80)90116-8

Woodhead, J., Eggins, S., and Gamble, J., 1993. High field strength and transition element systematics in island arc and back-arc basin basalts: evidence for multi-phase melt extraction and a depleted mantle wedge; Earth and Planetary Science Letters, v. 114, p. 491–504. doi:10.1016/0012-821X(93)90078-N

Geological Survey of Cananda Project 2001 333106 NP22